Identification of environmental and genetic factors important for *Cryptococcus neoformans* titan cell formation using new *in vitro* inducing conditions

Benjamin Hommel,[1,2,8,9] Liliane Mukaremera,[3,*] Radames J. B. Cordero,[4,*] Christopher A. Desjardins,[5,*] Aude Sturny-Leclère,[1,2,*] John Perfect,[6] James A. Fraser,[7] Arturo Casadevall,[4] Christina A. Cuomo,[5] Françoise Dromer,[1,2] Kirsten Nielsen,[3] Alexandre Alanio[1,2,8,9]

[*] These authors participated equally to the work

[1] Institut Pasteur, Molecular Mycology Unit, Paris, France
[2] CNRS URA3012, Paris, France
[3] Department of Microbiology and Immunology, University of Minnesota, Minneapolis, Minnesota, USA
[4] Department of Molecular Microbiology and Immunology, Johns Hopkins Bloomberg School of Public Health, Baltimore, MD.
[5] Broad Institute of MIT and Harvard, Cambridge, Massachusetts, USA
[6] Division of Infectious Diseases, Department of Medicine, Duke University Medical Center, Durham, North Carolina, USA
[7] Australian Infectious Diseases Research Centre, The University of Queensland, Brisbane, Queensland, Australia
[8] Laboratoire de Parasitologie-Mycologie, Hôpital Saint-Louis, Groupe Hospitalier Lariboisière, Saint-Louis, Fernand Widal, Assistance Publique-Hôpitaux de Paris (AP-HP), Paris, France
[9] Université Paris Diderot, Sorbonne Paris Cité, Paris, France

Corresponding Author: Alexandre Alanio, Molecular Mycology unit, Institut Pasteur, 25 rue du Dr Roux 75724 Paris Cedex 15; email: alexandre.alanio@pasteur.fr; Tel: +33140613255; Fax: +33145688420

Abstract

A remarkable aspect of the human fungal pathogen *Cryptococcus neoformans* is the morphological changes triggered by the interaction with the host. During infection, a specific morphological change in cell size is observed, particularly in lung tissue, from regular 5 to 7 µm cells (RCs) to titan cells (TCs, > 10 µm and up to 100 µm). However, the stable and reproducible generation of large quantity of TCs was only possible during experimental infection. We implemented here *in vitro* conditions allowing TCs generation with the aim to understand the ancestry of TC, the environmental determinants of TCs formation and perform easily phenotype/genotype analysis to uncover genetic factors underlying TCs formation.

This paper reports robust *in vitro* conditions that generates yeasts cells harboring the main characteristics of TCs: large (>10 µm), uninucleate and polyploid cells harboring a single large vacuole with a dense capsule surrounding a thickened melanized cell wall. We observed that TCs formation begins as soon as 8 hours after induction, with a maximal proportion of TCs obtained after 24 hours. TCs derived for the initial oldest cells (mother cells) rather than from daughter cells. Hypoxia, nutrient starvation and low pH stresses were the main factors that trigger TCs formation, while quorum sensing factors like the initial inoculum concentration and the addition of pantothenic acid also impacted TCs formation. Antifungal drugs, resulting in inhibition of ergosterol (fluconazole), or proteins and nucleic acids (flucytosine), altered TCs formation, as did hosts-related products such as serum, phospholipids and anti-capsular antibodies in our settings. We then explored genetic factors important for TCs formation using two approaches. Using strains from H99 lineage strains among which few genetic differences have been described, we showed that TCs formation was dependent on Lmp1, Sgf29 and Gpr4/5-Rim101 proteins. Then, based on a the analysis of natural Pkr1 loss-of-function clinical

52 isolates and serial clinical isolates, we observed the important role of Pkr1 protein, a negative
53 regulator of the cyclic adenosine monophosphate / protein kinase A (cAMP/PKA), for TCs
54 formation. These strains also emphasize the structural and functional relationship between
55 Pkr1 and Pka.
56 Our results provide new insights into TCs biogenesis with identification of multiple important
57 factors/pathways involved. The implementation of such standardized and robust *in vitro*
58 conditions pave the way for future research focusing on the genetic basis of TCs biogenesis,
59 biology of TCs and the ontology of morphological changes in *Cryptococcus neoformans*.
60
61

Author Summary:

Cryptococcus neoformans is a yeast that is capable of morphological change upon interaction with host. Particularly, in the lung of infected mice, a subpopulation of yeast evolves toward gigantism (titan cells size from 10 to 100 µm) that include other characteristics such as thickened cell wall, dense capsule, polyploidization, large vacuole with peripheral nucleus and cellular organelles. The generation of large number of such cells outside the lung of mice have been described but was not reproducible nor standardized. We here report standardized, reproducible, robust conditions of generation of titan cells and explored the environmental and genetic factors underlying the genesis of these cells. We showed that Titan cells were generated upon stresses such as change in the medium, nutrient deprivation, hypoxia and low pH. Using collection of well characterized reference strains and clinical isolates, we validated with our model the AMPc/PKA/Rim pathway as the major genetic determinant of titan cell formation. This study opens the way for a more comprehensive picture of the ontology of morphological changes in *Cryptococcus neoformans*.

76 **Introduction**

77

78 The ubiquitous environmental yeast *Cryptococcus neoformans* (Cn) is a
79 basidiomycetous yeast that causes up to 223,000 incident cases of meningoencephalitis and
80 more than 181,000 deaths per year worldwide [1], occurring mostly in immunocompromised
81 individuals with acquired immunodeficiency syndrome (AIDS) [2]. The natural history of most
82 of the cases of this invasive fungal infection proceeds through 3 stages: (i) primary infection
83 via inhalation of desiccated yeasts or basidiospores, with development of sub-clinical
84 pneumonia and spontaneous resolution via granuloma formation; (ii) latency of dormant
85 yeast cells, as demonstrated epidemiologically [3] and biologically [4] and (iii) reactivation and
86 dissemination upon immunosuppression, with meningoencephalitis as the main clinical
87 presentation [5]. From environment to interaction with hosts, the yeasts experience drastic
88 changes that require a capacity to rapidly adapt and survive in host tissues and cause disease
89 [4,6–9]. In hosts, Cn is exposed to various stresses including high temperature, nutrient
90 deprivation, low pH, hypoxia and high levels of free radicals [10].

91 In response to the host environment, morphological changes are required to survive
92 and cause disease [11]. Specifically, Cn alter its morphology and produce enlarged cells
93 referred to as giant or "titan cells" [12,13]. This phenomenon has been observed in animal and
94 insect models of cryptococcosis, as well as in human lung and brain infections [12–16]. The
95 titan cells (TCs) have increased cell body size, ranging from 10 µm to up to 100 µm in diameter
96 [13,17–21] as compared to the 5-7 µm size of regular cells (RCs). Studies exploring TCs biology
97 have revealed that these are: (i) uninucleate polyploid cells harboring a (ii) large single vacuole
98 surrounded by a (iii) thick cell wall and (iv) a dense and highly crosslinked capsule [17]. TCs
99 also exhibit increased resistance to various stresses including phagocytosis [21], oxidative and

100 nitrosative stress [20,21], and resistance to the antifungal drug fluconazole [20]. Importantly,
101 TCs production also enhances dissemination, survival and virulence in a mouse model of
102 infection [19]. TCs formation is known to be regulated by the G-protein coupled receptors
103 Gpr5 and Ste3a, that signal through the Gα subunit protein Gpa1 to trigger the cyclic
104 adenosine monophosphate / protein kinase A (cAMP/PKA) signaling pathway [15,20,22–25].
105 The cAMP/PKA pathway is critical for regulation of other virulence factors in Cn, including
106 capsule formation [22,23], notably through its action on the ubiquitin-proteasome pathway
107 [26]. Pka1 is known to be tuned by a regulatory protein Pkr1, and *pkr1Δ* mutant strains exhibit
108 enlarged capsule [22]. Further studies show TCs formation is increased by high *PKA1*
109 expression or low Pkr1 activity and is decreased by low *PKA1* expression [6]. Downstream of
110 the PKA pathway, Rim101, a major transcription factor that again controls production of many
111 virulence factors, is also necessary for TCs production [18].

112 To date, studies of TCs formation have been hindered by an inability to consistently
113 and reproducibly generate large quantities of TCs *in vitro*. Although several methods have
114 been reported for inducing large cell *in vitro* there have been persistent problems in easily and
115 consistently implementing these protocols across laboratories [17], presumably because the
116 variables that contribute to inducing conditions are not well understood.

117 In this study, we developed robust *in vitro* conditions that generates enlarged cells with
118 many of the *in vivo* TCs characteristics and used this protocol to explore environmental and
119 genetic factors involved in TCs formation. The genetic determinants of TCs formation have
120 been investigated through a genotype-phenotype correlation study based on the H99
121 laboratory reference strains and clinical isolates and validated by adequate KO mutants.

Results

Titan cells generated *in vitro* had similar characteristics to *in vivo* titan cells

While growth in minimal medium (MM) using standard growth conditions has no effect on cell size, we identified growth conditions that stimulate production of enlarged yeasts cells and optimized this experimental protocol, referred to as the Titan Cell Generating (or TCG) protocol, using our H99O reference strain (Fig 1). Observation of these *in vitro*-generated large cells by microscopy shows many characteristics of TCs including increased cell body size (diameter >10 µm), thicker refractive cell wall, large central vacuole, and peripheral cell cytoplasm distribution (Fig 2A). The TCG protocol was reproducible, with H99O reference strains generating equivalent proportions of TCs in three different laboratories throughout the world (Fig 2B). Specifically, the proportion of TCs was 39.4% [interquartile range (IQR), 34.1-40.7] in lab 1, 21.0% [12.5-26.8] in lab 2 and 29.9% [23.1-48.5] in lab 3.

TCs differ from regular cells (RCs) in various characteristics including capsule size melanization, cell wall structure and DNA content. TCs exhibit pronounced melanization, measured as blackness on the pictures, compared to RCs (Fig 2C, S1 Fig), with a median of the (max - mean grey intensity per pixel) of 20065 [18785-21887] in TCs vs. 13067 [9660-15998] in RCs ($p<0.0001$). TCs exhibit a slight but significant increase in capsule size compared to RCs (median 3.4 µm in large cells vs. 3.1 µm in RC, $p<0.001$, Fig 2D). Capsule structure was analyzed based on binding pattern (fluorescence intensity and distribution) of four monoclonal antibodies specific for capsular polysaccharides [27] (S2 Fig), and no pronounced difference between the capsule structures of TCs and RCs was quantified although some differences could be observed. Chitin content was significantly increased in TCs compared to RCs as determined by calcofluor white (CFW) fluorescence intensity (fluorescence intensity/pixel/cell

146 87.9 [71.7-107.7] vs. 66.5 [51.7-79.4], respectively, $p<0.0001$, Fig2E, S2 Fig). Finally, chitin
147 levels assessed by N-acetylglucosamine content determined by a biochemical method were
148 also higher in TCs (156.3 mM/g [153.7-203.7]) than in RCs (97.7 [87.2-119.3]), ($p<0.001$, Fig2F).
149 Cell sorting based on CFW staining and fluorescence microscopy allowed us to validate that
150 cells exhibiting the higher CFW intensity were TCs (FSC/SSC^{high}, S3 Fig).

151 To analyze DNA content, yeasts obtained at the end of the TCG protocol were stained
152 with propidium iodide (PI), with fluorescence in TCs (FSC/SSC^{high}) and RCs (FSC/SSC^{low})
153 compared to haploid (H99O) and diploid (AD7-77) strains grown in Sabouraud medium. DNA
154 content was higher in TCs (FSC/SSC^{high}) than RCs (FSC/SSS^{low}) cells (Fig 2G), with an increase in
155 the number of TCs cells with PI fluorescence > 2C (Fig 2H). In contrast, the RCs cells had the
156 same PI fluorescence pattern as the haploid H99O cells. Similarly, a reverse gating strategy
157 based on PI intensity shows yeasts with the highest PI intensity were large TCs cells (red
158 arrows, S4 Fig).

159

160 **TCs develop from older cells and produce regular daughter cells**

161 To examine temporal changes in cell size with the TCG protocol, we measured yeast
162 cell sizes at 0, 4, 8, 16, 24 and 120 h using automated analysis with the Icy software. This
163 automated analysis correlated with manual size measurements (Interclass correlation=0.99)
164 and TC/RCs classification (Kappa test=0.81±0.07). The median cell size increased during the
165 first 24 h of incubation, starting at 5.7 µm [5.4-6.0] and increasing to 9.7 µm [8.4-11.0] (Fig
166 3A). The first TCs cells were observed at 8 h with a progressive increase in the proportion of
167 TCs overtime, reaching a plateau by 24 h (Fig 3B).

168 Temporal changes in cell morphology where determined using live cell imaging and
169 light microscopy. Cells with the large vacuole characteristic of TCs appeared between 4 and 8

170 hours (Fig 3C, white arrow). Live cell imaging over 18 h (Supplemental material 1) showed that:
171 (i) TCs swelled from an older (parental) RCs and (ii) TCs produced RCs daughter cells. Calcofluor
172 white (CFW) staining was transferred to daughter cells upon division [4,28] and was used to
173 further monitor the ancestry of TCs and RCs cell populations over time using flow cytometry
174 (Fig 3D). The initial CFW stained population (0 h) consisted of RCs (FSC/SSC^{low}) cells with high
175 CFW fluorescence intensity. At 24 h, TCs (FSC/SSC^{high}) had high CFW fluorescence intensity,
176 indicating these cells were in the original CFW stained population. The RCs (FSC/SSC^{low}) cells
177 were composed of two populations: i) cells with high CFW intensities from the original stained
178 population and ii) daughter cells with low CFW intensity (Fig 3D left panel) indicating these
179 were new daughter cells. Direct comparison of cell size (FSC) and CFW intensity at 24 h (Figure
180 3D, right panel) showed the FSC^{high} cells (TCs) had a higher CFW fluorescence intensity (black
181 arrow) suggesting that they represent the older progenitor mother cells while the H24 FSC^{low}
182 cells (RCs) had lower CFW fluorescence intensity suggesting these were newly formed
183 daughter cells (white arrow). These combined data show that the TCs cells derived from the
184 initial inoculated cells and produced regular-sized RCs cells upon cell division.
185
186 **Generation of TCs *in vitro* is influenced by environmental conditions**
187 We tested several parameters affecting steps 2 and 3 of the TCG protocol described in
188 Fig 1 and identified changes that significantly influence TCs generation as measured by cell
189 size distribution and TCs proportion ($p<0.0001$). The first parameter we tested was the growth
190 medium and transition between different growth mediums (Fig 4A). Initial culture in YPD (step
191 2) and transfer to MM (step 3) had the highest median cell size at 9.1 µm [6.9-11.1]. Culture
192 from MM to MM produced fewer TCs, 25.5% (118/463) vs. 39.5%(182/461), although the TCs
193 tended to be larger with diameters over 20 µm. Light exposure during step 3 also increased

194 both median cell size and proportion of TCs (Fig 4B). In the light, median cell size was 9.4 µm
195 [7.3-11.4] vs. 8.4 µm [7.1-9.9] in the dark, with a TCs proportion at 41.6% (983/2362) vs. 24.3%
196 (1072/4399), respectively (Fig 4B). Incubation temperature at 30°C at step 3 increased cell size
197 distribution compared to 37°C (9.4 µm [7.3-11.4] vs. 7.0 µm [6.2-8.2]) as well as the proportion
198 of TCs (41.6% (983/2362) vs. 8.1% (297/3652)) (Fig 4C). The pH of the MM at step 3 also
199 influenced cell size (Fig 4D), with pH=5.5 producing significantly larger cells that (9.1 µm [6.9-
200 11.2] and 38.6% of TCs), compared to either lower pH (pH=4: median 5.1 µm [4.4-5.8] (0%
201 TCs)) or higher pH (pH=7: 8.2 µm [7.2-9.4] (16.4% TCs), or pH=8.5: 6.9µm [5.9-7.9] (0.7% TCs))
202 (Fig 4D). Finally, hypoxia at step 3 also increased median cell size compared to normoxia (7.5
203 µm [5.9-9.7]), with chemically induced hypoxia yielding higher median cell sizes compared to
204 physically induced hypoxia] (10.1 µm [7.8-12.5] vs. 8.9 µm [7.3-10.9, $p<0.0001$) (Fig 4E). The
205 proportion of TCs in normoxia (14.5% (732/5050) was lower than in chemically induced
206 hypoxia or physically induced hypoxia (63.0% (732/1161) and 38.6% (1264/3004),
207 respectively) ($p<0.0001$).
208
209 **Generation of TCs *in vitro* is influenced by fungal and host derived cues**
210 Previous studies of titan cell formation in a murine pulmonary infection model showed
211 that inoculum concentration can impact titan cell production [12,13]. To explore this
212 phenomenon, we examined cell size changes in response to different initial concentrations of
213 cells at step 3 (Fig 5A). Inoculated cell concentration significantly impacted the median cell
214 size of the yeast population ($p<0.0001$), with the highest median cell size observed at
215 10^6cells/mL (9.2 [7.3-11.1]) compared to 10^5 cells/mL (6.3 [5.1-8.3]), 10^4 cells/mL (6.2 [5.1-
216 7.9]) and 10^7 cells/mL (5.9 [5.2-6.5]) (Fig 5A). Similarly, the proportion of TCs generated was
217 significantly higher at 10^6 cells/mL (37.6% (896/2382) compared to 10.3% (279/2716) at 10^4

218 cells/mL, 14.3% (346/2420) at 10^5 cells/mL and 0% at 10^7 cells/mL (0/2177), p<0.0001.
219 Previous studies reported vitamin B5 (pantothenic acid) is involved in quorum sensing *C.*
220 *neoformans* [29]. The addition of vitamin B5 to the TCG protocol had no effect on median cell
221 size (8.35 µm [6.9-10.2] and 8.3 µm [6.4-10.8], p=0.8011, Fig 5B), but significantly increased
222 the proportion of TCs (37.9% (1435/3785) vs. 26.9% (983/3650)). Recent studies also implicate
223 the role of the small Qsp1 peptide by *C. neoformans* cells in quorum sensing [30]. Addition of
224 Qsp1 peptide significantly decreased median cell size from 9.1 µm [7.1-11.2] to 8.5 µm [6.9-
225 10.1] (Fig 5C) and TCs proportion from 38.4% (1075/2798) to 26.6% (915/3439), p<0.0001.
226 We then tested hosts factors that could interact *in vivo* with yeasts cells in the lung such as
227 anticapsular antibodies, serum and phosphatidylcholine, which both have already been shown
228 to help producing TCs *in vitro* [13,18,31]. Monoclonal antibodies co-incubated at step 3 that
229 bind to different epitopes of the capsule inhibited TCs generation, with a decreased cell size
230 of 7.2 µm [6.1-8.3] for E1 mAb, and 6.8 µm [5.9-7.7] for 18B7 mAb compared to the untreated
231 control (8.9 µm [7.1-10.6]) (Fig 5D), with a significantly smaller proportion of TCs (3.2%
232 (44/1360) with 18B7, 5.3% (67/1273) with E1 compared to 33.1% (327/987) for the control).
233 The addition of fetal calf serum (FCS) significantly decreased median cell size (7.3 µm [6.4-8.1]
234 vs. (9.1 µm [7.1-11.1], Fig 5E) and the proportion of TCs (2.5% (99/3911) vs. 38.2%
235 (1234/3228), p<0.0001) compared to control, as did the addition of phosphatidylcholine (PC)
236 (8.0 µm [7.0-9.0] vs. 9.0 µm [7.1-11.2] for the median cell size, (Fig 5F) and the proportion of
237 TCs (14.7% (344/2340) vs. 38.2% (1077/2820), p<0.0001).
238 To understand if the alteration of the metabolism induced by antifungal drugs affected TCs
239 formation, we tested the effect of co-incubation of fluconazole (inhibitor of ergosterol
240 synthesis) and flucytosine (inhibitor of nucleic acids formation and transcription) at step 3.
241 Fluconazole (FLC) exposure during step 3 resulted in significantly smaller median cell sizes

242 compared to control (7.1 µm [6.2-8.3]) at 1mg/L (data not shown), 6.8 µm [5.9-7.8] at 2 mg/L
243 (data not shown), and 6.5 µm [5.6-7.2] at 4 mg/L vs. 9.4 µm [7.5-11.3] in the control, Fig 5G)
244 and a significantly smaller proportion of TCs (5.9% (124/2073) at 1 mg/L, 2.9% (55/1919) at 2
245 mg/L and 1.0% (19/1877) at 4 mg/L vs. 40.9% (877/2146) in the control, $p<0.0001$). Flucytosine
246 exposure also significantly decreased the mean cell size at all concentrations tested (6.5 µm
247 [5.9-6.9] at 1 mg/L, 6.5 µm [6.1-6.9] at 2.5 mg/L, and 6.4 µm [5.9-6.8] at 5 mg/L compared to
248 control (8.3 µm [6.8-10.3], Fig 5H) with no TCs observed upon flucytosine exposure. Of note,
249 the viability of the cells recovered at step 4 after 5 days of drug exposure was unchanged for
250 fluconazole but reduced for flucytosine ($p<0.0001$ compared to unexposed, S5 Fig). We then
251 were interested to test if iterative subcultures with or without the presence of active
252 molecules (CFW or fluconazole) would affect TCs formation, assuming that the cell wall and
253 the global metabolism of the sub-cultured progeny would be impaired in the presence of high
254 concentration of cell wall toxic drug (CFW) or fluconazole, respectively. So, we analyzed the
255 impact of repeated sub-culture of the cells prior to step 1 on TCs cell production (Fig 5I). Sub-
256 culture on Sabouraud agar 8 times (8Sub) spanning a one-month period decreased
257 significantly the median cell size (8.60 µm [7.02-10.07]) compared to the initial culture (0Sub)
258 (9.17 [6.99-10.90]) ($p<0.0001$). Addition of CFW to induce cell wall stress during sub-cultures
259 (8Sub+CFW) had no significant impact on median cell size (8.03 µm [6.82-9.46]) compared to
260 the 8Sub control. However, iterative exposure to fluconazole during sub-culture increased
261 significantly median cell size to 10.15 µm [8.04-13.23] (8Sub+FLC) compared to the 8Sub
262 control ($p<0.001$, Fig 5I).
263
264 ***In vitro* TCs generation is dependent upon genetic background and involves functional**
265 **abolition of the *LMP1* or *SGF29* genes.**

266 Previous whole genome sequencing studies identified single-nucleotide
267 polymorphisms (SNPs) and insertions/deletions (indels) between the H99 strains recovered
268 from various laboratories (Table 1) [32]. To determine whether any of these SNPs or indels
269 affect TCs generation, we tested the H99S, H99W, H99 CMO18, H99L, KN99α strains in the
270 TCG assay. H99O produced more TCs than the other H99-derived strains, p<0.0001 (Fig 6A, S6
271 Fig). These H99 derivative strains were also tested for their titan cell formation in the lungs of
272 infected mice (Fig 6B). As with *in vitro* TCs production, all the H99 derivative strains showed
273 lower levels of titan cell formation in the mouse model when compared to H99O (p<0.0001),
274 with the exception of KN99α that had equivalent titan cell production as H99O (Fig 6B).
275 Two genes, *LMP1* and *SGF29*, are dramatically affected by SNPs/indels in the H99
276 derivatives; *LMP1* has a frameshift deletion (H99W and H99 CMO18) and *SGF29* is deleted
277 (KN99 and H99L). To determine if these genes are involved in TCs production, we analyzed
278 *lmp1Δ* and *sgf29Δ* deletion mutants for *in vitro* TCs and *in vivo* titan cell formation (Fig 6C and
279 Fig 6D, respectively). The *sgf29Δ* mutant in the H99O background manifested halved TCs
280 generation from 8.1% (49/600) to 4.2% (25/600) (p<0.0001). The same mutant in H99S
281 manifested no TCs generation. We observed similar results for *lmp1Δ* with no TCs formation
282 in the *lmp1Δ* mutant. Complementation of *lmp1Δ* using the *lmp1Δ:LMP1* H99S strain restored
283 TCs generation to that found in H99S (Fig 6C). Importantly, the same trend was observed for
284 *in vivo* titan cell formation. The *sgf29Δ* mutant in H99O background reduced titan cell
285 formation from 18.8% (113/600) to 9.3% (37/400) (p<0.0001). The *lmp1Δ* H99S mutant had
286 only 3.5% (21/600) titan cell formation compared to 14% for H99S (84/600), p<0.0001, and
287 this decrease in titan cell formation was restored in the *lmp1Δ:LMP1* H99S strains (9.5%
288 (57/600)) (Fig 6D).
289

290 ***In vitro* TCs generation requires signaling through the Gpr/PKA/Rim101 pathway in both**
291 **laboratory reference strains and clinical isolates.**
292 The signal transduction pathway Gpr/PKA/Rim101 is known to regulate TCs formation *in vivo*
293 [18]. Briefly, the G coupled protein receptor 5 and Ste3a signals through Gpa1 to trigger
294 cAMP/PKA with downstream the Rim101 transcription factor. This pathway regulates
295 virulence factors such as capsule or melanin [33,34].
296 To determine if this same pathway was similarly critical for TCs generation *in vitro*, we
297 examined cell enlargement in the *gpr4Δ*, *gpr5Δ*, *gpr4Δ/gpr5Δ, rim101*Δ mutants and their
298 complemented strains in both the H99 and KN99α genetic backgrounds (Fig 7A, S6E Fig).
299 Rim101 function was similar to that observed *in vivo*, with little TCs generation in the rim101Δ
300 mutant (1.9% (51/2600)) and full restoration of TCs generation in the complemented strain
301 (9.2% (239/2600) as compared to the H99O control (11.0% (176/1600) ($p<0.0001$). Similar to
302 *in vivo* titan cell production, the *gpr4Δ/gpr5Δ* had no TCs generation, but surprisingly both of
303 the single *gpr4Δ* and *gpr5Δ* mutants also lacked TCs generation. Unlike *in vivo* titan cell
304 production, TCs generation in the *gpr4Δ/gpr5Δ* double mutant was not rescued by GPR5 alone
305 (Fig 7A). Taken together, these data suggest that signaling through both Gpr4 and Gpr5 via
306 Rim101 is required for TCs generation *in vitro*.
307 To determine whether the Gpr/PKA/Rim101 pathway can impact TCs generation in
308 clinical isolates, we also screened a total of 56 clinical isolates for their ability to produce TCs.
309 Two isolates (AD2-06a and AD2-02a) produced an increased proportion of TCs relative to
310 H99O (ratio of clinical strain/H99O of 2.78 and 1.62, respectively). Three additional isolates
311 (AD4-37a, AD1-95a, AD4-43a) were able to produce TCs but less than H99O (ratio=0.40, 0.23,
312 0.12, respectively). The proportion of TCs recorded for the other clinical isolates was close to

313 zero (ratio between 0.1 and 0.01% for five, less than 0.01% for six, and no TCs at all for the
314 remaining 39) (Fig 7B).

315 The complete genome sequence was obtained for 29 of the 56 clinical isolates and a
316 phylogenetic tree of these strains and the H99O reference strain shows high genetic diversity
317 (Fig 7C, Table 2). Compared to H99O, the high TCs generating strain AD2-06a harbored 31,229
318 SNPs and was closely related to AD3-55a (31,171 SNPs) and AD3-41a (28,599 SNPs), which
319 were both unable to produce TCs. A total of 19 genes were considered disrupted in AD2-06a
320 and not in AD3-55a and AD3-41a (S2 Table). Duplication of chromosomal regions have been
321 observed in the French sequenced clinical isolates (S3 Table) with AD2-06a harboring a large
322 duplication of chromosome 9 (Chr9, region 465 – 665kb). To assess whether the Chr9
323 duplicated region could be responsible for TCs formation, we explored a larger collection of *C.*
324 *neoformans* strains with complete genome sequence [35] and discovered five additional
325 clinical isolates (Ug2459, CCTP20, FFV14, WM-148, WM-626) harboring partial duplications on
326 chr9 duplication (Fig S7). We analyzed TCs generation in these 5 isolates, but only the Ug2459
327 strain generated TCs *in vitro* and in a low proportion (S7 Fig).

328 AD2-06a was isolated from the initial cerebrospinal fluid (CSF) sample of an HIV-
329 infected patient at diagnosis of cryptococcal meningitis. Another isolate, AD2-07, was
330 recovered from the CSF of the same patient after 13 days of amphotericin B treatment. Thus,
331 AD2-06a and AD2-07 are closely related with only 137 different SNPs and 40 indels. AD3-55a
332 is in the same clade and also very similar with 370 different SNPs and 64 indels (Fig 7C, 7D). In
333 contrast, these three isolates differ from H99O by 29,000 SNP and 3,386 indels. AD2-07 and
334 AD3-55a were both unable to produce TCs (Fig 7B), allowing a more fine-tuned analysis of
335 SNPs in these closely related strains that could explain the variable TCs generation observed
336 between the strains (Fig 7B).

337 Comparison of the AD2-06a, AD2-07, and AD3-55a genomes identified four genes with
338 loss-of-function mutations in AD2-06a but not in AD2-07 or AD3-55a: CNAG_00570 (PKR1) (Fig
339 7E), CNAG_07475 (hypothetical protein), CNAG_01240 (hypothetical protein) and
340 CNAG_05335 (hypothetical protein). More precisely, AD2-06a had a frameshift mutation at
341 glycine 124 in the CNAG_00570 (*PKR1*) leading to a truncated protein of 138 amino acids (Fig
342 7E).

343 Pkr1 is the cAMP-dependent protein kinase regulatory subunit that interacts with Pka
344 to regulate the phosphorylation activity of Pka. We identified that *PKR1* harbored a wild type
345 sequence in AD2-07, together with a dramatic decrease in TCs generation. In details, the
346 proportion of TCs generated AD2-07 was 1.0% (31/3047) compared to AD2-06a (39.1%,
347 (639/1633)) and H99O (15.2% (304/2001)), ($p<0.0001$). The median cell size of AD2-07 was
348 significantly decreased compared to AD2-06a and H99O (5.9 µm [5.2-6.6] for AD2-07, 8.5 µm
349 [7.0-13.0] for AD2-06a, and 7.7 µm [6.5-9.2] for H99O, $p<0.0001$, S8 Fig).

350 We then selected additional and already sequenced clinical isolates (S4 Table) that harbored
351 mutations leading to Pkr1 truncation at different levels (Bt156, Bt58, 8-1, Bt77, Bt117,
352 Ug2462) [36]. Specifically, a frameshift mutation at amino acid 14 with a stop introduced at
353 96 for Bt156, and a stop codon introduced at 130 for 2-06a, at 258 for Bt58, at 302 for 8-1, at
354 439 for Bt77, at 441 for Bt117, and at 445 for Ug2462 was observed (Fig 7E, Table 3). We
355 hypothesized that the strains with highly impacted/truncated Pkr1 protein would produce
356 more TCs. These strains were then tested using the TCG protocol together with AD2-06a. The
357 two largest truncations were observed in AD2-06a and Bt156. These two strains had high level
358 of TCs generated with a ratio of 2.8±1.0 for AD2-06a and 1.3±0.6 for Bt156 compared to H99O
359 (Fig7F), and a % of TC of 39.1% (639/1633) (median 8.5µm [7.0-13.0]) and 17.9% (469/2614)
360 (median 7.7µm [6.4-9.4]), respectively (Fig S8). For the other strains, the ratio and the

361 proportion of TCs generated and the median size was less than that of H99O: 0.2±0.0, 3.6%
362 (89/2464) and 6.9µm [6.0-7.8] for 8-1 strain; 0.2±0.1, 2.9% (110/3834) and 6.5µm [5.8-7.1] for
363 Bt77; 0.1±0.0 0.9% (27/3081) and 6.4µm [5.7-7.2] for Bt117; and 0.1±0.1, 1.5% (54/3628)
364 5.4µm [4.7-6.1] for Ug2462, p<0.0001) (Fig 7F, S8 Fig).
365 We then tested the ability of *pkr1Δ* in a KN99α background to generate TCs compared to
366 KN99α and H99O, and found that the *pkr1Δ* ratio was at 1.1±0.2 compared to the parental
367 strain KN99 α 0.0±0.0. The *pkr1Δ* median cell size (8.1 µm [6.7-9.5]) exceeded that of KN99α
368 (6.4 µm [5.5-7.2]) without reaching the level of H99O (8.7 µm [7.1-10.2]), p<0.0001 (data not
369 shown). And, TCs proportion was at 28.8% (207/719) for H99O, 1.0% (12/1179) for KN99α and
370 20.4% (191/935) for *pkr1Δ* (p<0.0001, Fig 7G).
371

372 **Discussion**

373

374 We identified and validated a new protocol allowing robust generation of TCs *in vitro*.
375 This protocol was discovered serendipitously while testing conditions that could induce
376 dormancy in Cn [4]. We observed yeast cell enlargement under defined growth conditions,
377 then optimized those conditions for TCs generation. It is important to note that the utility of
378 other published protocols to generate TCs *in vitro* were hindered by issues with inter-
379 laboratory reproducibility [13,31]. To establish the inter-laboratory transferability of our
380 protocol it was independently tested in two laboratories (K. Nielsen and A. Casadevall) and
381 the protocol produced equivalent results in all laboratories. Interestingly, TCs generation *in*
382 *vitro* was also observed by Ballou et al., 2017, using a different set of growth conditions (Ballou
383 et al., companion paper). Exploration of the similarities and differences between these
384 protocols will likely identify the critical environmental conditions that trigger titan cell
385 production *in vivo*.

386 TCs obtained *in vitro* exhibit many of the characteristics of *in vivo* titan cells recovered
387 from the lungs of infected mice [17]. Similar to previous work on *in vivo* titan cells, we defined
388 TCs as having a cell body size > 10 µm and RCs with a cell body size ≤ 10µm [12,13,18,21].
389 Melanization was increased in TCs compared to RCs and capsule size was slightly increased in
390 TCs compared to RCs but less than previously shown *in vivo* [12,13]. In addition,
391 immunofluorescence staining with 4 different antibodies showed no major difference
392 between the TCs and RCs capsule structure, indicating a conservation of polysaccharide
393 epitopes consistent with similar structures. The difference in melanization and capsule size
394 between TCs and RCs underscore the ability and the complexity of the regulation of these
395 virulence factors, leading to an adaptation of Cn to stress conditions, including hosts.

396 The cell wall was clearly thicker in TCs than in RC, with an increased chitin content
397 (determined both by increased CFW intensity and GlcNAc content). Increased CFW staining
398 and GlcNAc levels are also increased in *in vivo*-derived titan cells [30]. Finally, TCs generated
399 with our protocol were also polyplods, as previously shown *in vivo* [10,11].

400 TCs generation *in vitro* allowed a detailed kinetic analysis that revealed TCs start
401 forming in as little as 8 h, compared to 24 h for *in vivo* TCs [12,13]. Using our CFW method to
402 follow cell fate and cell division [4,28], we showed that the TCs were exclusively derived from
403 cells present in the initial inoculum that evolved progressively toward a TCs phenotype. In
404 contrast, the RCs were likely to be a mixture of cells from the initial inoculum and progeny of
405 cell division. TCs cell division produced regular-sized haploid RC, as shown previously for *in*
406 *vivo* titan cells [12,13]. We published *in vivo* data that validate this observation [4]. Indeed,
407 Calcofluor^{High} Cn population were associated with yeasts cells harboring high cell size
408 parameters using multispectral imaging flow cytometry of yeasts recovered from the lung of
409 infected mice 7 d after inoculation of Cn stained with calcofluor [4].

410 TCs generation coincided with the appearance of a large vacuole in the yeasts cells at
411 4 and 8 h of incubation. Recent evidence places vacuoles at the center of networks enabling
412 nutrient resources to be degraded, sorted and redistributed. As the vacuole volume occupies
413 much of the total volume of the TCs body size, one can imagine that cell-cycle regulation could
414 be impacted, ultimately leading to polyploidy [37].

415 The fact that *in vitro* protocol consistently produced TCs allowed us to test factors that
416 influenced their generation. In terms of environmental factors, we showed that TCs
417 generation was impacted by pre-culture medium, initial pH, light exposure, temperature, type
418 of medium and hypoxia. A metabolic switch between YPD pre-culture and MM incubation was
419 a key factor to induce TCs generation. This switch is a stress that induces a lot of metabolic

420 modifications and has been studied extensively in *Saccharomyces cerevisiae* [38]. Hypoxia is
421 another stress factor in human pathogenic fungi [39]. A major transcriptional regulator of the
422 fungal hypoxia response is the sterol regulatory element-binding protein (Srebp) [40]. Null
423 mutants of the Srebp (*sre1Δ*) in Cn display defects in adaptation to hypoxia, ergosterol
424 synthesis, susceptibility to triazole antifungal drugs and cause a reduction of virulence [41]. As
425 hypoxia was an important factor for TCs generation, whether Srebp is involved in TCs
426 formation needs to be determined. Also, oxygen levels in healthy human tissues are 20–70
427 mmHg (2.5–9% O_2), and can be less than 10 mmHg (~1% O_2) [42]. We know from previous
428 work on pulmonary aspergillosis that hypoxia have been observed in infected lungs of mice
429 [43]. Titan cells have been reported in human pulmonary cryptococcosis and well-studied in
430 murine pulmonary infection following inhalation [13,17–21], although they are also observed
431 in mouse lungs after intravenous inoculation of animals [4]. These observations lead us to
432 hypothesize that low oxygen levels in the lungs could be one of signals that trigger titan cell
433 formation.

434 Interestingly, quorum sensing is also involved in TCs generation. Indeed, the initial
435 concentration of yeasts in MM dramatically impacted TCs generation, with 10^6 cells/mL as the
436 optimal cell concentration (no TCs formation at 10^7 cells/mL). The addition Qsp1 peptide
437 [30,44] at step 3 to wild type H99O yeasts (already producing Qsp1) decreased TCs
438 generation, suggesting Qsp1 regulation may be important for sensing the population size.
439 Finally, pantothenic acid (vitamin B5) [29] had little impact on TCs generation by producing
440 more TC in proportion. These results show that intercellular communication is important for
441 the yeast to switch to the TCs phenotype and that this sensing process may involve cell-cell
442 communication instead of simply sensing nutrient levels. A relationship between stress

443 sensing and quorum sensing could be hypothesized based on our results and needs to be
444 further explored.

445 Host factors such as temperature, addition of lipids, presence of serum, and antibodies
446 were also tested. The presence of E1 [45] and 18B7 [46] anti-capsular IgG antibodies
447 decreased TCs generation. This decrease could be related to changes in the yeast metabolism
448 induced directly by anti-capsular antibodies as shown previously [47] and provide a new
449 mechanism by which antibodies could alter the course of infection. One could imagine that
450 specific anti-Cryptococcus anti-capsular antibodies could not diffuse locally in the lung as
451 compared to other organs. The presence of surfactant protein-D considered as an opsonin in
452 the lung could impair antibody fixation [48], thus inhibiting the inhibition effect of IgG
453 antibodies allowing at the end TC formation in the lung. The ability of capsule-binding
454 antibodies to interfere with TCs formation suggests another mechanism by which humoral
455 immunity could contribute to protection. Interestingly, addition of serum (FCS 5%) or L-α-
456 phosphatidylcholine decreased TCs generation, which is different from other protocols for TCs
457 generation [31] Balou et al. Companion paper]. This difference could be explained by the fact
458 that we developed a set of inducing conditions based on specific stresses that induce TCs
459 through parallel or independent pathways to those triggered by serum or lipids. Overall these
460 results imply the existence of numerous triggers for TCs formation mediated through
461 independent signaling pathways that can potentially interfere with each other.

462 The impact of antifungal drugs was also tested. Fluconazole is known to inhibit the 14-alpha-
463 demethylase (Erg11) involved in ergosterol synthesis, leading to plasma membrane instability
464 and accumulation of toxic precursors [49]. Flucytosine is a nucleoside analogue leading to
465 inhibition of DNA replication and protein synthesis [50]. TCs generation was clearly inhibited
466 by the addition of fluconazole or flucytosine even at concentrations that are below the MIC of

467 the strain. These data suggest TCs generation may be an active process requiring normal
468 protein and DNA replication processes, as well as plasma membrane integrity. Conversely,
469 stressing the yeast by serial passage on fluconazole agar (8 sub-cultures) led to increased TCs
470 generation, that assess that pre-activation of yeasts in specific conditions (YPD, fluconazole
471 exposure) are required for TC formation. In other experimental settings, exposure of TCs to
472 fluconazole selected for aneuploidy in the daughter cells [20]. Of note, exposure to cell-wall
473 stress induced by serial passage on CFW agar, decreased TCs generation and suggests that
474 intact cell wall metabolism is required for TCs generation. In these sub-culturing experiments,
475 we did not investigate subsequent genomic or metabolic changes that arise under these stress
476 conditions. Serial sub-culture could have induced genetic rearrangements (aneuploidy, SNPs,
477 indels) or epigenetic variation that could explain the altered TCs generation and can be
478 explored further in future studies.

479 Our TCG protocol is practical for studying molecular and genetic mechanisms
480 underlying TCs generation. The TCG protocol allowed us to identify host, environmental and
481 yeast factors that impact TCs generation. By taking advantage of strains harboring few genetic
482 differences (H99 strains or AD2-06a and AD2-07), the TCG protocol is also a powerful tool to
483 assess genetic factors modulating TCs generation, as shown with *SGF29*, *LMP1*, and *PKR1*.
484 Sgf29, is a transcription factor that binds H3K4me2/3 and recruits histone deacetylation in *S.*
485 *cerevisae* [51]. *LMP1* gene is known to be involved in virulence in mouse model and mating
486 [32]. It is clear that these genes are required for TCs generation, although their mechanism of
487 action remains unclear. We also reproduced *in vitro*, the role of the Gpr/PKA/Rim101 pathway
488 in TCs formation previously observed *in vivo* [18]. Gpr5 signals through Gpa1 to trigger the
489 PKA pathway that activates the transcription factor Rim101 [18,33]. Altogether, these results
490 are a proof of concept that the TCG protocol can be used to identify and characterize genes

491 required for TCs generation. We still only know a handful of genes involved in TCs generation
492 and it is likely are large number of genes are involved in generation of this complex cell
493 morphology.

494 Analysis of differences in TCs generation, combined with complete genome
495 sequencing, allowed us to identify naturally occurring mutations in the *PKR1* gene that impact
496 TCs generation. Pkr1 is part of the cAMP/PKA pathway previously shown to modulate titan
497 cell formation *in vivo* [52]. The Pkr1 protein is known as the regulator of Pka activity [22]. The
498 pathway is responsible of cell cycle regulation in *S. cerevisae* and in *Xenopus* oocytes [53,54].
499 We tested the *pkr1Δ* mutant (CNAG_00570) from the Madhani deletion collection and it
500 produced 20-fold more TCs than the parental KN99α strain, corroborating the regulatory role
501 of Pkr1 on Pka, and the role of Pka in yeast morphogenesis. Interestingly, a *PKR1* mutation
502 was identified in an incident clinical isolate (AD2-06a). Surprisingly, the recurrent isolate
503 recovered following 13 d of amphotericin B treatment (AD2-07) did not have this *PKR1*
504 mutation. This could be indirect evidence that *PKR1* loss of function impacts the fitness of the
505 strain under amphotericin B treatment. Interestingly, *PKR1* mutation leading to intron
506 retention was found in a relapse isolate [55] and shown to be less virulent than the incident
507 isolate. Whether the virulence observed with the relapse isolates is linked to TCs formation
508 needs to be further investigated. In *Saccharomyces cerevisiae* the Pka1/Pkr1 complex is a
509 heterotetramer with 2 catalytic subunits and 2 regulatory units. This complex is dissociated in
510 the presence of cAMP [56]. Moreover, the architecture of the functional domains of *Pkr1*
511 include one interaction domain/dimerization at amino acids 2 to 40 and two cAMP binding
512 domains at amino acids 219 to 351 and 353 to 473, based on INTERPRO data (Fig 7E).
513 Consequently, PKA1/PKR1 complex dissociation is critical for binding of cAMP on the Pka1
514 domain. Interestingly, two distinct naturally occurring *PKR1* mutations were identified in the

515 clinical strains that all impacted TCs formation by reducing the protein length by introducing
516 a stop codon (Gly125fs for AD2-06 and Asp14fs for Bt58).

517 Altogether, these results are a proof of concept that the TCG protocol can be used
518 to identify and characterize genes required for TCs generation. We still only know a handful
519 of genes involved in TCs generation and it is likely that large number of genes are involved in
520 generation of this complex cell morphology. Our data provide new insight into the genesis of
521 TCs and into the environmental, host and genetic factors that influence the generation of TCs.
522 Our data show that our *in vitro* assay can be used to reproducibly generate TCs that have
523 similar characteristics to titan cells generated *in vivo*. The conditions identified for TCs
524 formation provide a robust system that could be invaluable to dissect the molecular
525 mechanisms that underlie TCs formation and allowed the identification of naturally occurring
526 mutations that regulate TCs formation.

527 **Material and methods**

528

529 **Ethics statement**

530 Mice (purchased from Jackson Laboratories, Bar Harbor, ME) were handled in accordance with
531 guidelines defined by the University of Minnesota Animal Care and Use Committee (IACUC),
532 under approved protocol numbers 1010A91133 and 130830852. All animal experiments were
533 performed in concordance with the Animal Welfare Act, United States federal law, and NIH
534 guidelines.

535

536 **Strains and culture medium**

537 The strains and clinical isolates of *C. neoformans* (Cn) used in the study are listed in S1 Table.
538 The study was started with H99 strain called H99O that was kindly provided by J. Heitman
539 (Duke University, Durham, NC) in the late 90's. Strains from the Madhani collection were
540 provided from the Fungal Genetic Stock Center [57].

541 Cn strains were grown in liquid Yeast Peptone Dextrose (YPD, 1% yeast extract (BD Difco, Le
542 pont de Claix, France) 2% peptone (BD difco), 2% D-glucose (Sigma, Saint Louis, Minnesota,
543 USA)) and in minimal medium (MM, 15mM D-glucose (Sigma), 10 mM $MgSO_4$ (Sigma), 29.4mM
544 KH_2PO_4 (Sigma), 13mM Glycine (Sigma) , 3.0 µM Thiamine (Sigma), [29]). Minimum inhibitory
545 concentration (MIC) of H99O for fluconazole (FLC) and flucytosine (5FC) (both purchased from
546 lsachim, Shimadzu Group Company, Illkirch-Graffenstaden, France) were determined by the
547 EUCAST method and were 8 and 4 mg/L, respectively.

548

549 ***In vitro* protocol for TCs generation (TCG protocol)**

550 Cn strain from stock cultures stored in 20% glycerol at -80°C was cultured on Sabouraud agar
551 plate at room temperature (step 1). After 2 to 5 d of culture, approximately 10^7 cells were
552 suspended in 10mL YPD in a T25cm^3 flask and cultured 22 h at 30°C, 150 rpm with lateral
553 shaking until stationary phase (final concentration=2x10^8cells/mL) (step 2). Then, one mL of
554 the suspension was washed twice with MM. The cell concentration was adjusted to 10^6
555 cells/mL in MM and the suspension was incubated in a 1.5 mL tube (Eppendorf) with the cap
556 closed, at 30°C, 800 rpm for 5 d using an Eppendorf Thermomixer® (Hambourg, Germany)
557 (step 3). Cell size was determined as described below. Cells with body size >10 µm were
558 considered as TCs as described [12]. Results are expressed as median cell size [interquartile
559 range, IQR] or as median [IQR] of the % of TCs in a given condition for H99 or as a ratio
560 compared to %TCs obtained with the H99O in experiments involving other strains (clinical
561 isolates, other H99 strains and mutants).
562
563 **Capsule size analysis and melanization**
564 Yeasts were observed after India ink staining and capsule size was determined as described
565 below using the following formula: whole cell size - cell body size)/2.
566 Capsule immunofluorescence (IF) of TCs was done by incubating approximately 5x10^6 cells/mL
567 with 10µg/mL of murine-derived monoclonal antibodies to the cryptococcal capsule (IgG1
568 18B7, IgG1 E1, IgM 12A1, IgM 2D10 [27,45,58,59] in blocking solution (1% bovine serum
569 albumin in PBS). Cells and mAb mixtures were done in 1.5 mL microcentrifuge tubes at 37 °C
570 for 1 h under continuous mixing. Next, cells were washed three times with PBS by
571 centrifugation (5,000 rpm for 5 mins at room temperature) and incubated for 1 h at 37 °C with
572 5 µg/mL fluorescently labelled secondary-mAbs, goat anti-mouse IgG1-FITCs or IgM-TRITCs
573 (Southern Biotech) in blocking solution and 1 µg/mL of Uvitex2b (Polysciences, Warrington,

574 PA) solution to visualize the fungal cell wall. Cells were washed three times with PBS by
575 centrifugation, mounted in glass coverslips and imaged with an Olympus AX 70 microscope
576 equipped with blue, green and red fluorescent filters using 40x and/or oil immersion 100x
577 objectives. Capsule IF of TCs preparations performed in two independent experiments gave
578 consistent results.
579 TCs melanization was induced following step 3. Cells were washed once with MM, suspended
580 in 1mL of MM supplemented with 1mM of L-DOPA (Sigma D9628), transferred to a 5mL
581 Erlenmeyer flask (for normal oxygenation) and incubated at 30 °C under continuous mixing at
582 200 rpms for 3 days. Since melanin is resistant to acid hydrolysis, a spherical melanin "ghost"
583 remains following incubation of black cells with 12N HCl for 1 h at 100 °C (a reduced and
584 modified version of the procedure in [60]. Acid-resistant melanin "ghosts" were washed three
585 times in PBS by centrifugation and visualized using light microscopy.
586 Melanization was measured using imageJ in Icy software by manually circling each cell and
587 measuring the mean gray intensity / pixel /cell. Blackness was calculated as the maximum
588 mean grey intensity minus the mean gray intensity / pixel /cell. Increasing melanin content
589 will result in higher blackness. As melanization darkened the cells, the most darkened cells
590 were the less intense the mean gray was.
591
592 **Chitin density quantification**
593 Chitin density was determined after calcofluor white staining (CFW, fluorescent brightener 28)
594 adapted from [37]. Briefly, 10^7 Cn cells in 10 mL MM were washed once and 500 µl of 3.7%
595 formaldehyde in PBS was added. Cells were incubated at room temperature for 30-40
596 minutes, inverting the tube every 5 minutes. Samples were washed twice in PBS, cell
597 concentration was adjusted to 10^6 cell/ml. The supernatant was removed and 1 mL of 0.01

598 µg/mL CFW in PBS was added, and incubated 5 minutes at 25°C. Cells were then washed twice
599 in PBS. Results were expressed as median [IQR] of the mean fluorescence intensity/pixel/cell
600 after picture analysis as described below.
601
602 **N-acetylglucosamine quantification/ Chitin measurement**
603 H99KN cells were grown in MM for 48 h *in vitro*. Cells were centrifugated 2 min at 14,000 and
604 were then washed twice with sterile water. These cells were exposed to γ-radiation to remove
605 layers of the capsule polysaccharide [13]. Cells resuspended in sterile water were transferred
606 to a 24-well flat-bottom plate and irradiated for 45 min: dose 560 Gy (56,000 rad).
607 TCs and RCs populations were separated [20]. Washed irradiated cells were filtered using
608 CellMicroSieves (BioDesign Inc. of New York, Carmel, NY) with a 10 µm pore size. The
609 CellMicroSieves were rinsed with PBS to remove RCs from the filter. To recover the TCs
610 population, the CellMicroSieves were inverted and the membrane was washed with PBS. The
611 TCs population was concentrated by centrifugation at 12,000 g for 1 min. To recover the RCs
612 population, the filter flow-through was concentrated by centrifugation at 12,000 g for 1 min.
613 Cellular chitin quantification was adapted from [61]. Purified *in vitro* RCs and TCs were
614 collected by centrifugation at 14,000 rpm for 2 min and the media were removed. Dry weights
615 were measured following 2-3 d of evaporation at 37°C. Dried pellets were extracted with 1 ml
616 6% KOH at 80°C for 90 min. Samples were centrifuged at 14,000 rpm for 20 min. Each pellet
617 was suspended in 1 ml PBS and spun again. Each pellet was suspended in 0.2 ml of McIlvaine's
618 Buffer (0.2 M Na2HPO4, 0.1 M citric acid, pH 6.0). Five µL of purified *Streptomyces griseus*
619 chitinase (5 mg/mL in PBS) was added to hydrolyze chitin to GlcNAc and were incubated for 3
620 d at 37°C. Chitinase-treated samples were spun at 14,000 rpm for 1 min, each 10 µL of sample
621 supernatant was combined with 10 µL 0.27 M sodium borate, pH 9.0. Samples were heated

622 to 99.9°C for 10 min. Upon cooling to room temperature, 100 µl of DMAB solution (Ehrlich's
623 reagent, 10 g p-dimethylaminobenzaldehyde in 12.5 mL concentrated HCl, and 87.5 ml glacial
624 acetic acid) was added, followed by 20 min incubation at 37°C. Hundred µL was transferred to
625 96-well plates, and absorbance at 585 nm was recorded. Standard curves were prepared from
626 stocks of 0.2 to 2.0 mM of GlcNAc (Sigma, Saint Louis, Missouri, USA). The amount of GlcNAc
627 was calculated as mmol/g cells (dry weight). Results are expressed as median [IQR].
628

629 **DNA content measurement**

630 A 96-well microtiter plate was filled with 200 µL of a 10^6/mL cell suspension in PBS and
631 centrifuged 5 minutes at 4000 rpm. The pellet was suspended in 150 µL of ethanol 70% and
632 incubated in the dark 1 h at 4°C. After discarding the supernatant, a 50 µL mix composed of
633 44 µL NS (0.01M Tris HCL pH 7.2, 1 mM EDTA, 1mM CaCl2, 0.25 M Sucrose, 2.12 mM $MgCl_2$,
634 0.1 mM $ZnCl_2$), 5µL RNase A at 10mg/mL and 1.25µL PI at 0.5mg/mL was added in each well
635 as described [62]. After a 30 minutes' incubation at 30°C in the dark, the plate was sonicated
636 1 minute and each sample diluted at 1:40 in 50mM Tris HCl. The fluorescence intensity was
637 measured using the Guava easyCyte 12HT Benchtop Flow Cytometer® (Guava, MERCK,
638 Kenilworth, New Jersey). Selection of singlets by gating allowed (i) determination of PI
639 intensity on channel YelB (583/26) in FSC/SSC^{high} (TCs) and FSC/SSC^{low} (RCs); (ii) determination
640 of the FSC/SSC distribution in PI^{high} and PI^{low} population. FlowJo software v.10 was used to
641 analyze the data. The graphs of the number of yeasts were normalized to the mode to depict
642 the data in terms of '% of max'. The % of max denotes the number of cells in each bin (the
643 numerical ranges for the parameter on the *x* axis) divided by the number of cells in the bin
644 that contains the largest number of cells.
645

646 **Determination of the ancestry of TCs by flow cytometry**

647 Knowing that CFW staining does not alter Cn viability, and that daughter cells harbored lower
648 CFW signal due to partial cell wall transmission from mother to daughter cells [4,28], we
649 analyzed cell size and CFW fluorescence intensity of the progenies of TCs and RCs following
650 the TCG protocol on 10^6 cells of H99O pre-stained with CFW (channel BluV 448/50 using
651 Guava).

652

653 **Dynamic imaging**

654 Cell size evolution over time was assessed for strain AD2-06a by dynamic imaging (Nikon
655 Biostation). Briefly, 35 mm sterile culture dish (Hi-Q4, Nikon) were coated for 1 min with E1
656 antibody at 2 mg/L in order to provide anchor for the capsule. Yeasts (10^5 cells) were added
657 in 1 mL MM and incubated at 32°C for 18 h. Series of 221 images were taken by phase-contrast
658 microscopy every 5 mins at ×100 magnification. Merging was done using ImageJ software in
659 Icy Software.

660

661 **Impact of various factors on TCs generation**

662 To analyze the various factors that could impact TCs generation, we modified the various steps
663 of the TCG protocol. For step1, stress was produced by 8 subcultures (twice a week for one
664 month) on agar medium or on agar supplemented with CFW (20mg/L) or with fluconazole
665 (32mg/L). For step 2, the pH of MM (normally at 5.5) was set at 4, 7 or 8.5 without buffering.
666 For step 3, initial cell concentration (from 10^4 to 10^7cells/mL) was tested. Hypoxia was
667 generated physically by closing the cap of the Eppendorf® tube during 5 d or chemically upon
668 incubation in MM supplemented with 1 nM $CoCl_2$, cap closed, as already described [63]. The
669 production of TCs was also assessed in the presence of various reagents added at step 3: (1)

670 Qsp1 peptide (NFGAPGGAYPW, [30]) (Biomatik, Cambridge, Canada) was resuspended at
671 10mM in water and stored at -80°C until use at 10 µM final ; (2) pantothenic acid purchased
672 from Sigma (Saint-Louis, Missouri, USA) used at 125 µM; (3) monoclonal anti-capsular
673 antibodies E1 [45] and 18B7 [46] used at a final concentration of 166 µg/mL in MM [64]; (4)
674 decomplemented fetal calf serum (FCS, Invitrogen, Carlsbad, CA, USA) at 5 % in MM; (5) L-α-
675 Phosphatidylcholine from egg yolk (Sigma, Saint-Louis, Missouri, USA) was extemporaneously
676 reconstituted at 5 mM in MM; (6) antifungal drugs (fluconazole and flucytosine) were tested
677 at the concentrations close to the MIC (2-fold dilutions) with the diluent (DMSO or water) as
678 control. Results are expressed as median [IQR]. Growth in the presence or in the absence of
679 antifungal drugs was evaluated by enumeration of yeasts cells concentration at step 4 of TCG
680 protocol using the Guava cytometer, starting from 10^6 cells inoculated at step 1.
681
682 **Production and isolation of TCs from infected mice**
683 Cn strains were cultured overnight at 30°C in YPD broth medium (BD, Hercules, Canada). Cells
684 were collected by centrifugation, washed with phosphate buffered saline PBS and
685 resuspended in sterile saline. Groups of 6- to 8-week-old C57BL/6J mice (Jackson Labs, Bar
686 Harbor, Maine) were anesthetized by intraperitoneal pentobarbital injection and infected
687 intranasally with 5×10^6 cells in a 50 µl volume. Infected mice were sacrificed by CO_2 inhalation
688 at 3 days post-infection. The lungs were harvested, homogenized, and then resuspended in
689 10 ml PBS supplemented with collagenase (1 mg/ml) [13]. Cell homogenates were incubated
690 for 1hour at 37°C with agitation, and washed several times with double distilled water. The Cn
691 cells were fixed with 3.7 % formaldehyde for 40 min, washed 3 times with sterile PBS, and
692 then resuspended in sterile PBS. The proportion of TCs and RCs were determined by

693 microscopy. Data presented were from 3 mice per strain, except for strains *sgf29Δ* in H99O,
694 H99S that had 2 mice per strain.
695
696 ***In vitro* susceptibility testing**
697 Minimal inhibitory concentrations (MICs) were determined for flucytosine and fluconazole
698 (Alsachim, Shimadzu Group Company, Illkirch-Graffenstaden, France) according to the
699 EUCAST method [65].
700
701 **DNA Sequencing, Variant identification, and Bioinformatic Analysis**
702 Genome DNA was adapted for Illumina sequencing using Nextera reagents. Libraries were
703 sequenced on an Illumina HiSeq to generate 101 base reads. most data was previously
704 described [36,66] and one additional isolate was newly sequenced for this study (AD2-07)
705 (NCBI SRA accession SRR5989089). Reads were aligned to the *C. neoformans* var. *grubii* H99
706 assembly (GenBank accession GCA_000149245.2 [32] using BWA-MEM version 0.7.12 [67].
707 Variants were then identified using GATK version 3.4 [68] , where indels were locally realigned,
708 haplotypeCaller was invoked in GVCF mode with ploidy = 1, and genotypeGVCFs was used to
709 predict variants in each strain. All VCFs were then combined and sites were filtered using
710 variantFiltration with QD < 2.0, FS > 60.0, and MQ < 40.0. Individual genotypes were then
711 filtered if the minimum genotype quality < 50, percent alternate allele < 0.8, or depth < 5.
712 Variants were then functionally annotated with SnpEff version 4.2 [69]. For phylogenetic
713 analysis, the 369,574 sites with an unambiguous SNP in at least one isolate and with ambiguity
714 in at most 10% of isolates were concatenated; insertions or deletions at these sites were
715 treated as ambiguous to maintain the alignment. Phylogenetic trees were estimated using
716 RAxML version 8.2.4 [70] under the GTRCAT model in rapid bootstrapping mode. For

717 determination of PKR1 architecture domains, the INTERPRO tool was used
718 (http://www.ebi.ac.uk/interpro/protein/J9VH50).
719
720 **Pictures analysis using Icy software and statistical analysis**
721 To increase the number of events analyzed in each condition tested/each parameter analyzed
722 (cell size, capsule size and chitin content), pictures of 3-5 fields were taken with an AxioCam
723 MRm camera (Carl Zeiss, Oberkochen) at x40 on interferential contrast microscope (DMLB2
724 microscope; Leica, Oberkochen). Image were then analyzed (for cell size and chitin content)
725 using Icy software v.1.9.2.1. (icy.bioimageanalysis.org) and a specific plugin (HK-Means plugin
726 (http://icy.bioimageanalysis.org/plugin/HK-Means) that allows analysis of multiple structures
727 from a bright field. Preliminary experiments were done to compare results obtained with Icy
728 to "manual" measurements by analyzing about 200 cells on the same pictures for 3
729 independent experiments. In subsequent experiments, results were pooled for a given
730 condition from 2 to 3 independent experiments after good reproducibility was assessed.
731 Statistical analysis was performed with STATA® software (College Station, Texas, v13.0). To
732 validate the cell size determination using the Icy software, the intraclass correlation
733 coefficient was calculated. The ability of the automated method to classify the Cn cells as TCs
734 or RCs compared to visual measurement was evaluated using the Kappa test [71]. To compare
735 TCs generation in the various conditions, non-parametric tests were performed using the
736 Kruskal-Wallis test for multiple comparisons or Mann Whitney test as required. GraphPad
737 Prism software (v.6) was used to generate graphs.
738
739
740

741 **Data access**

742 All sequence data from this study have been submitted to NCBI BioProject
743 (https://www.ncbi.nlm.nih.gov/bioproject) under accession number PRJNA174567.
744 The AD2-07 sequence is available in the NCBI SRA under the accession number SRR5989089
745 (https://www.ncbi.nlm.nih.gov/sra/SRR5989089/)

746

747 **Acknowledgments**

748 We thank Dr Tihana Bicanic, Shichina Kannmbath, Charles Giamberardino and Jennifer Tenor
749 who kindly provided specific clinical isolates. The authors want to thank Marie Desnos-Ollivier
750 for her help with Sanger sequencing, JL Tinevez for technical assistance in Biostation
751 experiments, Stéphane Dallongeville for help with Icy Software, Stevenn Volant for
752 biostatistics and Paul-Henri Commere for FACS analysis. We thank Quigly Dragotakes for
753 helping us determining cell and capsule sizes in specific experiments. The authors
754 acknowledge Hiten Madhani and member of his laboratory for the knockout collection that
755 have been made freely available ahead of publication to the scientific community.

756

757

758 **References**

759 1. Rajasingham R, Smith RM, Park BJ, Jarvis JN, Govender NP, Chiller TM, et al. Global burden
760 of disease of HIV-associated cryptococcal meningitis: an updated analysis. Lancet Infect
761 Dis. 2017;17: 873. doi:10.1016/s1473-3099(17)30243-8

762 2. Park BJ, Wannemuehler KA, Marston BJ, Govender N, Pappas PG, Chiller TM. Estimation
763 of the current global burden of cryptococcal meningitis among persons living with
764 HIV/AIDS. AIDS Lond Engl. 2009;23: 525–530. doi:10.1097/QAD.0b013e328322ffac

765 3. Garcia-Hermoso D, Janbon G, Dromer F. Epidemiological evidence for dormant
766 *Cryptococcus neoformans* infection. J Clin Microbiol. 1999;37: 3204–3209.

767 4. Alanio A, Vernel-Pauillac F, Sturny-Leclère A, Dromer F. *Cryptococcus neoformans* host
768 adaptation: toward biological evidence of dormancy. mBio. 2015;6: e02580-14.
769 doi:10.1128/mBio.02580-14

770 5. Chrétien F, Lortholary O, Kansau I, Neuville S, Gray F, Dromer F. Pathogenesis of cerebral
771 *Cryptococcus neoformans* infection after fungemia. J Infect Dis. 2002;186: 522–530.
772 doi:10.1086/341564

773 6. Choi J, Vogl AW, Kronstad JW. Regulated expression of cyclic AMP-dependent protein
774 kinase A reveals an influence on cell size and the secretion of virulence factors in
775 *Cryptococcus neoformans*. Mol Microbiol. 2012;85: 700–715. doi:10.1111/j.1365-
776 2958.2012.08134.x

777 7. Franzot SP, Mukherjee J, Cherniak R, Chen LC, Hamdan JS, Casadevall A. Microevolution of
778 a standard strain of *Cryptococcus neoformans* resulting in differences in virulence and
779 other phenotypes. Infect Immun. 1998;66: 89–97.

780 8. Hu G, Cheng P-Y, Sham A, Perfect JR, Kronstad JW. Metabolic adaptation in *Cryptococcus*
781 *neoformans* during early murine pulmonary infection. Mol Microbiol. 2008;69: 1456–
782 1475. doi:10.1111/j.1365-2958.2008.06374.x

783 9. Gerstein AC, Nielsen K. It's not all about us: evolution and maintenance of *Cryptococcus*
784 virulence requires selection outside the human host. Yeast. 2017;34: 143–154.
785 doi:10.1002/yea.3222

786 10. Brown SM, Campbell LT, Lodge JK. *Cryptococcus neoformans*, a fungus under stress. Curr
787 Opin Microbiol. 2007;10: 320–325. doi:10.1016/j.mib.2007.05.014

788 11. Wang L, Lin X. Morphogenesis in fungal pathogenicity: shape, size, and surface. PLOS
789 Pathog. 2012;8: e1003027. doi:10.1371/journal.ppat.1003027

790 12. Okagaki LH, Strain AK, Nielsen JN, Charlier C. Cryptococcal cell morphology affects host
791 cell interactions and pathogenicity. PLoS Pathog. 2010;6: e1000953.
792 doi:10.1371/journal.ppat.1000953

793 13. Zaragoza O, García-Rodas R, Nosanchuk JD, Cuenca-Estrella M, Rodríguez-Tudela JL,
794 Casadevall A. Fungal cell gigantism during mammalian infection. PLoS Pathog. 2010;6:
795 e1000945. doi:10.1371/journal.ppat.1000945

796 14. Love GL, Boyd GD, Greer DL. Large *Cryptococcus neoformans* isolated from brain abscess.
797 J Clin Microbiol. 1985;22: 1068–1070.

798 15. Cruickshank JG, Cavill R, Jelbert M. *Cryptococcus neoformans* of unusual morphology. Appl
799 Microbiol. 1973;25: 309–312.

800 16. García-Rodas R, Casadevall A, Rodríguez-Tudela JL, Cuenca-Estrella M, Zaragoza O.
801 *Cryptococcus neoformans* capsular enlargement and cellular gigantism during *Galleria*
802 *mellonella* infection. PloS One. 2011;6: e24485. doi:10.1371/journal.pone.0024485

803 17. Zaragoza O, Nielsen K. Titan cells in *Cryptococcus neoformans*: cells with a giant impact.
804 Curr Opin Microbiol. 2013;16: 409–413. doi:10.1016/j.mib.2013.03.006

805 18. Okagaki LH, Wang Y, Ballou ER, O'Meara TR, Bahn Y-S, Alspaugh JA, et al. Cryptococcal
806 titan cell formation is regulated by G-protein signaling in response to multiple stimuli.
807 Eukaryot Cell. 2011;10: 1306–1316. doi:10.1128/EC.05179-11

808 19. Crabtree JN, Okagaki LH, Wiesner DL, Strain AK, Nielsen JN, Nielsen K. Titan cell production
809 enhances the virulence of *Cryptococcus neoformans*. Infect Immun. 2012;80: 3776–3785.
810 doi:10.1128/IAI.00507-12

811 20. Gerstein AC, Fu MS, Mukaremera L, Li Z, Ormerod KL, Fraser JA, et al. Polyploid titan cells
812 produce haploid and aneuploid progeny to promote stress adaptation. mBio. 2015;6:
813 e01340-15. doi:10.1128/mBio.01340-15

814 21. Okagaki LH, Nielsen K. Titan cells confer protection from phagocytosis in *Cryptococcus*
815 *neoformans* infections. Eukaryot Cell. 2012;11: 820–826. doi:10.1128/EC.00121-12

816 22. D'Souza CA, Alspaugh JA, Yue C, Harashima T, Cox GM, Perfect JR, et al. Cyclic AMP-
817 dependent protein kinase controls virulence of the fungal pathogen *Cryptococcus*
818 *neoformans*. Mol Cell Biol. 2001;21: 3179–3191. doi:10.1128/MCB.21.9.3179-3191.2001

819 23. Nichols CB, Perfect ZH, Alspaugh JA. A Ras1-Cdc24 signal transduction pathway mediates
820 thermotolerance in the fungal pathogen *Cryptococcus neoformans*. Mol Microbiol.
821 2007;63: 1118–1130. doi:10.1111/j.1365-2958.2006.05566.x

822 24. Bahn Y-S, Jung K-W. Stress Signaling Pathways for the Pathogenicity of *Cryptococcus*.
823 Eukaryot Cell. 2013;12: 1564–1577. doi:10.1128/EC.00218-13

824 25. Hu G, Steen BR, Lian T, Sham AP, Tam N, Tangen KL, et al. Transcriptional Regulation by
825 Protein Kinase A in *Cryptococcus neoformans*. PLOS Pathog. 2007;3: e42.
826 doi:10.1371/journal.ppat.0030042

827 26. Geddes JMH, Caza M, Croll D, Stoynov N, Foster LJ, Kronstad JW. Analysis of the protein
828 kinase A-regulated proteome of *Cryptococcus neoformans* identifies a role for the

829 ubiquitin-proteasome pathway in capsule formation. mBio. 2016;7: e01862-15.
830 doi:10.1128/mBio.01862-15

831 27. Casadevall A, DeShaw M, Fan M, Dromer F, Kozel TR, Pirofski L a. Molecular and idiotypic
832 analysis of antibodies to *Cryptococcus neoformans* glucuronoxylomannan. Infect Immun.
833 1994;62: 3864–3872.

834 28. Alanio A, Desnos-Ollivier M, Dromer F. Dynamics of *Cryptococcus neoformans*-
835 macrophage interactions reveal that fungal background influences outcome during
836 cryptococcal meningoencephalitis in humans. mBio. 2011;2: e00158-11.
837 doi:10.1128/mBio.00158-11

838 29. Albuquerque P, Nicola AM, Nieves E, Paes HC, Williamson PR, Silva-Pereira I, et al. Quorum
839 sensing-mediated, cell density-dependent regulation of growth and virulence in
840 *Cryptococcus neoformans*. mBio. 2013;5: e00986-13. doi:10.1128/mBio.00986-13

841 30. Homer CM, Summers DK, Goranov AI, Clarke SC, Wiesner DL, Diedrich JK, et al.
842 Intracellular action of a secreted peptide required for fungal virulence. Cell Host Microbe.
843 2016;19: 849–864. doi:10.1016/j.chom.2016.05.001

844 31. Chrisman CJ, Albuquerque P, Guimarães AJ, Nieves E, Casadevall A. Phospholipids trigger
845 *Cryptococcus neoformans* capsular enlargement during interactions with amoebae and
846 macrophages. PLoS Pathog. 2011;7: e1002047. doi:10.1371/journal.ppat.1002047

847 32. Janbon G, Ormerod KL, Paulet D, Byrnes EJ, Yadav V, Chatterjee G, et al. Analysis of the
848 genome and transcriptome of *Cryptococcus neoformans* var. *grubii* reveals complex RNA
849 expression and microevolution leading to virulence attenuation. PLoS Genet. 2014;10:
850 e1004261. doi:10.1371/journal.pgen.1004261

851 33. O'Meara TR, Alspaugh JA. The *Cryptococcus neoformans* capsule: a sword and a shield.
852 Clin Microbiol Rev. 2012;25: 387–408. doi:10.1128/CMR.00001-12

853 34. Cordero RJB, Casadevall A. Functions of fungal melanin beyond virulence. Fungal Biol Rev.
854 2017;31: 99. doi:10.1016/j.fbr.2016.12.003

855 35. Rhodes J, Desjardins CA, Sykes SM, Beale MA, Vanhove M, Sakthikumar S, et al. Tracing
856 genetic exchange and biogeography of *Cryptococcus neoformans* var. *grubii* at the global
857 population level. Genetics. 2017; doi:10.1534/genetics.117.203836

858 36. Desjardins CA, Giamberardino C, Sykes SM, Yu C-H, Tenor JL, Chen Y, et al. Population
859 genomics and the evolution of virulence in the fungal pathogen *Cryptococcus neoformans*.
860 Genome Res. 2017;27: 1207–1219. doi:10.1101/gr.218727.116

861 37. Wiesner DL, Specht CA, Lee CK, Smith KD, Mukaremera L, Lee ST, et al. Chitin recognition
862 via chitotriosidase promotes pathologic type-2 helper T cell responses to cryptococcal
863 infection. PLoS Pathog. 2015;11: e1004701. doi:10.1371/journal.ppat.1004701

38. Zhang N, Cao L. Starvation signals in yeast are integrated to coordinate metabolic reprogramming and stress response to ensure longevity. Curr Genet. 2017; doi:10.1007/s00294-017-0697-4

39. Nizet V, Johnson RS. Interdependence of hypoxic and innate immune responses. Nat Rev Immunol. 2009;9: 609–617. doi:10.1038/nri2607

40. Grahl N, Shepardson KM, Chung D, Cramer RA. Hypoxia and fungal pathogenesis: to air or not to air? Eukaryot Cell. 2012;11: 560–570. doi:10.1128/EC.00031-12

41. Chun CD, Liu OW, Madhani HD. A link between virulence and homeostatic responses to hypoxia during infection by the human fungal pathogen *Cryptococcus neoformans*. PLoS Pathog. 2007;3: e22. doi:10.1371/journal.ppat.0030022

42. Lewis JS, Lee JA, Underwood JC, Harris AL, Lewis CE. Macrophage responses to hypoxia: relevance to disease mechanisms. J Leukoc Biol. 1999;66: 889–900.

43. Grahl N, Puttikamonkul S, Macdonald JM, Gamcsik MP, Ngo LY, Hohl TM, et al. In vivo hypoxia and a fungal alcohol dehydrogenase influence the pathogenesis of invasive pulmonary aspergillosis. PLoS Pathog. 2011;7: e1002145. doi:10.1371/journal.ppat.1002145

44. Lee H, Chang YC, Nardone G, Kwon-Chung KJ. TUP1 disruption in *Cryptococcus neoformans* uncovers a peptide-mediated density-dependent growth phenomenon that mimics quorum sensing. Mol Microbiol. 2007;64: 591. doi:10.1111/j.1365-2958.2007.05666.x

45. Dromer F, Salamero J, Contrepois A, Carbon C, Yeni P. Production, characterization, and antibody specificity of a mouse monoclonal antibody reactive with *Cryptococcus neoformans* capsular polysaccharide. Infect Immun. 1987;55: 742–748.

46. Zebedee SL, Koduri RK, Mukherjee J, Mukherjee S, Lee S, Sauer DF, et al. Mouse-human immunoglobulin G1 chimeric antibodies with activities against *Cryptococcus neoformans*. Antimicrob Agents Chemother. 1994;38: 1507. doi:10.1128/aac.38.7.1507

47. McClelland EE, Nicola AM, Prados-Rosales R, Casadevall A. Ab binding alters gene expression in *Cryptococcus neoformans* and directly modulates fungal metabolism. J Clin Invest. 2010;120: 1355–1361. doi:10.1172/JCI38322

48. Geunes-Boyer S, Beers MF, Perfect JR, Heitman J, Wright JR. Surfactant protein D facilitates *Cryptococcus neoformans* infection. Infect Immun. 2012;80: 2444–2453. doi:10.1128/IAI.05613-11

49. Sanglard D, Ischer F, Calabrese D, de Micheli M, Bille J. Multiple resistance mechanisms to azole antifungals in yeast clinical isolates. Drug Resist Updat. 1998;1: 255. doi:10.1016/s1368-7646(98)80006-x

50. Loyse A, Dromer F, Day J, Lortholary O, Harrison TS. Flucytosine and cryptococcosis: time to urgently address the worldwide accessibility of a 50-year-old antifungal. J Antimicrob Chemother. 2013;68: 2435–2444. doi:10.1093/jac/dkt221

901 51. Bian C, Xu C, Ruan J, Lee KK, Burke TL, Tempel W, et al. Sgf29 binds histone H3K4me2/3
902 and is required for SAGA complex recruitment and histone H3 acetylation. EMBO J.
903 2011;30: 2829–2842. doi:10.1038/emboj.2011.193

904 52. Kronstad JW, Attarian R, Cadieux B, Choi J, D'Souza CA, Griffiths EJ, et al. Expanding fungal
905 pathogenesis: *Cryptococcus* breaks out of the opportunistic box. Nat Rev Microbiol.
906 2011;9: 193–203. doi:10.1038/nrmicro2522

907 53. Duckworth BC, Weaver JS, Ruderman JV. G2 arrest in *Xenopus* oocytes depends on
908 phosphorylation of cdc25 by protein kinase A. Proc Natl Acad Sci U S A. 2002;99: 16794–
909 16799. doi:10.1073/pnas.222661299

910 54. Mitsuzawa H. Increases in cell size at START caused by hyperactivation of the cAMP
911 pathway in *Saccharomyces cerevisiae*. Mol Gen Genet MGG. 1994;243: 158–165.

912 55. Chen Y, Farrer RA, Giamberardino C, Sakthikumar S. Microevolution of serial clinical
913 isolates of *Cryptococcus neoformans* var. *grubii* and *C. gattii*. mBio. 2017;8: e00166-17.
914 doi:10.1128/mbio.00166-17

915 56. Vandamme J, Castermans D, Thevelein JM. Molecular mechanisms of feedback inhibition
916 of protein kinase A on intracellular cAMP accumulation. Cell Signal. 2012;24: 1610–1618.
917 doi:10.1016/j.cellsig.2012.04.001

918 57. McCluskey K, Wiest A, Plamann M. The Fungal Genetics Stock Center: a repository for 50
919 years of fungal genetics research. J Biosci. 2010;35: 119–126.

920 58. Casadevall A, Cleare W, Feldmesser M, Glatman-Freedman A, Goldman DL, Kozel TR, et al.
921 Characterization of a murine monoclonal antibody to *Cryptococcus neoformans*
922 polysaccharide that is a candidate for human therapeutic studies. Antimicrob Agents
923 Chemother. 1998;42: 1437–1446.

924 59. Mukherjee J, Casadevall A, Scharff MD. Molecular characterization of the humoral
925 responses to *Cryptococcus neoformans* infection and glucuronoxylomannan-tetanus
926 toxoid conjugate immunization. J Exp Med. 1993;177: 1105–1116.

927 60. Wang Y, Aisen P, Casadevall A. Melanin, melanin "ghosts," and melanin composition in
928 *Cryptococcus neoformans*. Infect Immun. 1996;64: 2420–2424.

929 61. Banks IR, Specht CA, Donlin MJ, Gerik KJ, Levitz SM, Lodge JK. A chitin synthase and its
930 regulator protein are critical for chitosan production and growth of the fungal pathogen
931 *Cryptococcus neoformans*. Eukaryot Cell. 2005;4: 1902–1912. doi:10.1128/EC.4.11.1902-
932 1912.2005

933 62. Tanaka R, Taguchi H, Takeo K, Miyaji M, Nishimura K. Determination of ploidy in
934 *Cryptococcus neoformans* by flow cytometry. J Med Vet Mycol Bi-Mon Publ Int Soc Hum
935 Anim Mycol. 1996;34: 299–301.

936 63. Ingavale SS, Chang YC, Lee H, McClelland CM, Leong ML, Kwon-Chung KJ. Importance of
937 mitochondria in survival of *Cryptococcus neoformans* under low oxygen conditions and

938 tolerance to cobalt chloride. PLoS Pathog. 2008;4: e1000155.
939 doi:10.1371/journal.ppat.1000155

940 64. McClelland EE, Ramagopal UA, Rivera J, Cox J, Nakouzi A, Prabu MM, et al. A Small protein
941 associated with fungal energy metabolism affects the virulence of *Cryptococcus*
942 *neoformans* in mammals. PLoS Pathog. 2016;12: e1005849.
943 doi:10.1371/journal.ppat.1005849

944 65. Arendrup MC, Cuenca M. Method for the determination of broth dilution minimum
945 inhibitory concentrations of antifungal agents for conidia forming moulds. 2014.

946 66. Rhodes J, Beale M, Vanhove M, Jarvis JN, Kannambath S, Simpson JA, et al. A population
947 genomics approach to assessing the genetic basis of within-host microevolution
948 underlying recurrent cryptococcal meningitis infection. G3 Genes. 2016;
949 doi:10.1101/083469

950 67. Li H. Aligning sequence reads, clone sequences and assembly contigs with BWA-MEM.
951 1303;

952 68. McKenna A, Hanna M, Banks E, Sivachenko A, Cibulskis K, Kernytsky A, et al. The genome
953 analysis toolkit: a mapReduce framework for analyzing next-generation DNA sequencing
954 data. Genome Res. 2010;20: 1297–1303. doi:10.1101/gr.107524.110

955 69. Cingolani P, Platts A, Lily Wang, Coon M, Nguyen T, Wang L, et al. A program for annotating
956 and predicting the effects of single nucleotide polymorphisms, SnpEff: SNPs in the genome
957 of *Drosophila melanogaster* strain w1118; iso-2; iso-3. Fly (Austin). 2012;6: 80–92.
958 doi:10.4161/fly.19695

959 70. Stamatakis A. RAxML version 8: a tool for phylogenetic analysis and post-analysis of large
960 phylogenies. Bioinforma Oxf Engl. 2014;30: 1312–1313.
961 doi:10.1093/bioinformatics/btu033

962 71. The Kappa Statistic in Reliability Studies: Use, Interpretation, and Sample Size
963 Requirements. Phys Ther. 2005; doi:10.1093/ptj/85.3.257

964

965 **Supporting informations**

966

967 **S1 Fig. TCs melanization.** Comparing the blackness of the cell body of TCs (white arrows) and
968 RCs upon melanization conditions showed that TCs contained more melanin than RCs.
969 (Bar=10µm).

970

971 **S2 Fig. Immunofluorescence staining with anti-capsular polysaccharide monoclonal**
972 **antibodies (mAbs) 2D10, 12A1, 18B7, E1 does not uncover major differences in capsular**
973 **structures between TCs (white arrows) and RCs (black arrows).** Each panel correspond to the
974 same cells observed after staining with (a) India ink; (b) calcofluor white; (c) one of the Mabs;
975 (d) merge from c and d. (bar=10µm).

976

977 **S3 Fig. The FSC^{high}/CFW^{high} population of yeasts correspond to TCs.** Cells obtained at the end
978 of the TGC protocol were stained with CFW and sorted by flux cytometry according to size
979 (FSC) and CFW fluorescence intensity (left panel). Sorted yeasts were observed using bright
980 field and fluorescence microscopy (right panel) (bar=10µm).

981

982 **S4 Fig. Among yeasts recovered at the end of the TCG protocol, those with the highest DNA**
983 **content have the bigger cell size.**
984 DNA content was analyzed after propidium iodide (PI) staining of yeast cells obtained at the
985 end of the TCG protocol (H99O TCG), in a control haploid strain (H99O cultured in Sabouraud
986 agar, H99O Sab) and in a control diploid strain (AD7-77 cultured in Sabouraud agar). Part of
987 the population of H99O TCG had a higher PI (blue arrow) fluorescence intensity than the
988 haploid control (upper panel). Gating on the PI intensity showed that the increase in the PI

989 fluorescence intensity from <20K to >40K corresponded to increase in cell size (FSC) (red
990 arrows) compared to the diploid (AD7-77) and haploid (H99O Sab) control (lower panel).
991
992 **S5 Fig. The yeasts growth is maintained in the presence of antifungals after TCG protocol.**
993 10^6 cell/mL were inoculated at step 1 of TCG protocol, then cell growth was evaluated by
994 enumerating cell concentration obtained at step 4 of TCG protocol using Guava flow
995 cytometer for cell counting. (**A**) Compared to control, fluconazole did not modify cell growth
996 in MM whereas (**B**) flucytosine (5FC) reduced it, when used at concentration near the
997 minimum inhibitory concentration (MIC) for 5 days (*p<0.0001 compared to unexposed
998 control). The fluconazole and flucytosine MICs for H99O were 8 mg/L and 4 mg/L, respectively.
999 Experiments were done in triplicates (bars represent mean ± SD).
1000
1001 **S6 Fig**. **TCs generation is dependent on various genes *in vitro* and *in vivo*.** (**A**) Strains from the
1002 H99 lineage harbored variable abilities to generate TCs with high TCs producer (H99O, S, L)
1003 and low TCs producer (KN99α, H99W, H99 CMO18) *in vitro* and (**B**) *in vivo* (except for KN99α)
1004 compared to H99O. (**C**) The *sgf29*Δ and *lmp1*Δ mutant strains show a decrease in TCs
1005 generation in various H99 backgrounds *in vitro* and (**D**) *in vivo* compared to H99O. (**E**) Rim
1006 pathway is required for TCs generation *in vitro* in H99. Each experiment was done in triplicates.
1007 Results are presented as stacked bar of the % of Titan cells (TCs) and regulars cells (RCs), *
1008 p<0.0001 vs. control H99O.
1009
1010 **S7 Fig. Chr9 ploidy does not influence TCs generation.** A panel of 7 clinical isolates with partial
1011 Chromosome 9 duplication (left panel) was tested for its ability to generate TCs. Only H99O
1012 and AD2-06a exhibited increased cell sizes (middle panel). The % of TC was 67.9 % (431/667)

1013 for 2-06a, 32.1% (429/1339) for H99O, and 4.2% (51/1227), for Ug2459 (Khi2 compared to
1014 H99O, *p<0.0001) with the % TCs ratio to that produced in H99O shown in the right panel.
1015
1016 **S8 Fig. *PKR1* mutations influence median cell size**
1017 Strains with *PKR1* loss of function mutation showed a variable ability to produce TCs
1018 depending on the resulting truncated proteins. The clinical isolate AD2-07 which did not
1019 harbor the *PKR1* mutation was recovered from the CSF of an HIV-positive patient on day 13 of
1020 amphotericin B treatment while AD2-06a was recovered from its initial CSF. The median cell
1021 size of AD2-07 (5.9 µm [5.2-6.6]) was significantly decreased compared to H99O (7.7 µm [6.6-
1022 9.2]) and 8.5 µm [7.0-13.0] for AD2-06a (p<0.0001). Except Bt156 (median of 7.7 µm [6.4-9.4]),
1023 the others strains had a significantly decreased median size compared to H99O (p<0.0001),
1024 6.9 µm [6.0-7.8] for 8-1 strain; 6.5 µm [5.8-7.1] for Bt77, 6.4 µm [5.7-7.2] for Bt117; and 5.4
1025 µm [4.7-6.1] for Ug2462. Experiments were done in triplicate and pooled.
1026
1027 **SI material 1: TCs generation begins between 8 and 12 h and TCs are able to produce yeasts**
1028 **with regular size.**
1029 Dynamic imaging of yeasts from the AD2-06a *C. neoformans* clinical isolate using the Nikon
1030 Biostation IM. Yeasts were seeded in MM on a culture dish that was previously coated with
1031 E1 at 2 mg/L. Images were taken every 5 min for 24 h at ×100 magnification using
1032 transmitted light (white bar=10µm)
1033
1034 **S1 Table: Strains used in this study**
1035

1036 **S2 Table: Gene disrupted in AD2-06a but not in closely related isolated AD3-55a or AD3-**

1037 **41a**

1038

1039 **S3 Table: Clinical isolates with chromosome 9 ploidy variation**

1040

1041 **S4 Table: Strains harboring Pkr1 loss-of-function mutations used in this study**

1042 **Figures and Tables**

1043

1044 **Fig 1. *In vitro* protocol of titan cells generation (TCG protocol).** The protocol followed several
1045 steps: (1) *C. neoformans* H99O from a frozen stock culture at -80°C was cultured on Sabouraud
1046 agar for 2-5 days; (2) Approximately 10^7 yeasts were then suspended in 10mL of liquid Yeast
1047 Peptone dextrose (YPD) and incubated under agitation (150 rpm) at 30°C for 22 h (stationary
1048 phase); (3) 1ml of the culture was then washed twice in minimal medium (MM), then 10^6
1049 yeasts were resuspended in 1mL of MM in a 1.5 mL Eppendorf® tube and incubated at 800
1050 rpm for up to 120 hours using an Eppendorf thermomixer; (4) A mixture of regular cells and
1051 of titan cells (TCs) was ready for analysis.

1052

1053 **Fig 2. Titan cells generated *in vitro* harbor the typical phenotype of titan cells produced *in***
1054 ***vivo*.**
1055 (**A**) Typical morphology of titan cells (TCs, white arrow) was observed (increased body size (a,
1056 > 10 µm), capsule (b), thickened cell wall, large central vacuole, and peripheral cell cytoplasm
1057 distribution) while the size of regular cells (RCs, black arrow) is <10 µm. (**B**) TCs were
1058 reproducibly generated in lab 1 using H99O and in two independent laboratories (lab 2 and
1059 lab 3) using their local H99O strain. Cell size was measured manually or by using the Icy
1060 software on pictures taken in bright field. Each dot represents an independent experiment
1061 (median [interquartile range, IQR] are presented); (**C**) Melanization was more intense in TCs
1062 than RCs (*p<0.0001) based on the calculation of the max - mean grey value/pixel of each
1063 melanin ghost measured (n=19 for TCs and n=531 for RCs) using the ImageJ in Icy software.
1064 Each dot represented an individual cells and boxes median and IQR (**D**) Capsule size measured
1065 after India ink staining was significantly larger in TCs than in RCs. Dots represent individual

1066 cells, and boxes median and IQR for 250 cells each (*p<0.001); (**E**) Chitin was denser in TCs
1067 than in RCs according to CFW fluorescence intensity/pixel/cell measured by Icy software after
1068 CFW staining (0.01 µg/ml) at step4 of the TCG protocol (*p<0.0001). Dots represent individual
1069 cells, and boxes median and IQR for 400 cells each (*p<0.001, pooled measurements from 3
1070 independent experiments); (**F**) N-acetylglucosamine (GlcNAc), the monomer component of
1071 chitin, was increased in TCs compared to RCs as measured by a biochemical method after
1072 gamma-irradiation of the yeasts to remove the capsule, allowing a better separation of TCs
1073 and RCs. Each dot represent result from independent experiments (n=7). Results are
1074 presented as median and IQR (p<0.001). (**G**) The yeasts recovered at step4 of the TCG protocol
1075 and analyzed by dot plots (FSC/SSC) using flow cytometry showed two populations FSC/SSC^{high}
1076 and FSC/SSC^{low} representing TCs and RC, respectively; (**H**) DNA content analysis after
1077 propidium iodide (PI) staining showed that the TCs (FSC/SSC^{high}) population harbored
1078 increased PI fluorescence intensity from 2C to >4C as compared to the diploid control (AD7-
1079 77 cultured in Sabouraud agar) while the RCs (FSC/SSC^{low}) population harbored a PI intensity
1080 comparable to the haploid control (H99O cultured in Sabouraud agar).
1081
1082 **Fig 3**. **Dynamics of TCs generation *in vitro***. (**A**) Cell body size was measured from samples of
1083 H99O culture (step 3 of the TCG protocol) withdrawn at specific times (H0 to H120) using
1084 pictures taken in bright field and measured with the ICY software (mean number of yeasts
1085 counted ± SD = 219 ± 67, representative of three experiments). Cell size increased starting at
1086 H8 with some cells reaching the threshold of 10 µm (grey dashed line). Each dot represents a
1087 single cell and the bars represent median and IQR; (**B**) TCs generation started between H8 and
1088 H12 and reached a plateau at H24. Each dot represents the proportion of TCs in the
1089 corresponding sample (3 independent experiments); (**C**) Pictures (x400 magnification) taken

1090 overtime showing the progressive increased in cell body size and the appearance of a vacuole
1091 typical of TCs in a large cell at H8 (white arrow) (scale bar 10 µm); (**D**) Cells stained with
1092 calcofluor (CFW) at 0.1 µg/mL prior to incubation using the TCG protocol. CFW fluorescent
1093 intensity is analyzed by flow cytometry in the initial (H0) and the resulting FSC/SSC^{high} (TCs)
1094 and FSC/SSC^{low} (RCs) observed at H24. The initial (H0) (green line) and the H24 FSC/SSC^{high}
1095 (blue line) populations harbored a high CFW fluorescence suggesting that they are mother
1096 cells, with a higher fluorescence for the FSC/SSC^{high}, while two populations of high and low
1097 (black star) CFW fluorescence intensity were observed for the H24 FSC/SSC^{low} cells (Left panel).
1098 The right panel shows the size (FSC) and CFW fluorescence intensity of the yeast populations
1099 at H0 (black density lines) and H24 (yellow density lines). The initial population
1100 (CFW^{high}/FSC^{low}) evolved in two populations, one corresponding to daughter cells (RC,
1101 CFW^{low}/FSC^{low}, white arrow), and the other one corresponding to TCs (CFW^{high}/FSC^{high}, black
1102 arrow).
1103
1104 **Fig 4. TCs generation *in vitro* is impacted by various environmental conditions**. (A) The
1105 sequence of media used at steps 2 and 3 of the TCG protocol was crucial for TCs generation:
1106 yeasts cultured in YPD and transferred to minimal medium (MM) produced significantly more
1107 TCs (cells >10µm, dotted grey line) than yeasts cultured in MM or YPD and transferred in MM
1108 or YPD, respectively; (B) Exposure to day light at step 3 had a positive impact on TCs generation
1109 compared to incubation in the dark; (C) Raising the incubation temperature to 37°C at step 3
1110 decreased TCs formation compared to 30°C; (D) Modification of the initial pH of the MM used
1111 at step 3 modifies TCs formation with pH 5.5 being optimal while a more acidic (pH=4), a
1112 neutral (pH=7) or an alkaline (pH=8.5) pH inhibited TCs formation; (E) The impact of hypoxia
1113 was tested by physical (closed cap) and by chemical ($COCl_2$ in MM at 1 nM) method and

1114 compared to normoxia (21% oxygen). Physically- and chemically-induced hypoxia enhances
1115 the production of TCs compared to normoxia with a higher proportion of TCs in physically-
1116 compared to chemically-induced hypoxia. All experiments were performed in triplicate and
1117 pooled (mean cell counted ± SD =2305±1438). Median and IQRare shown in black for each
1118 condition (* p<0.0001 vs. reference condition, grey circled dots). The percentages above each
1119 condition represents the % of TCs observed.

1120

1121 **Fig 5. Titan cells generation *in vitro* is influenced by quorum sensing factors, host factors**
1122 **and antifungal drugs.** (**A**) The cell concentration at onset of step2 significantly modified TCs
1123 generation with a maximal TCs formation using an initial concentration of 10^6 cells/mL, and an
1124 abolition of TCs formation at 10^7 cells/mL; We then tested several factor at step 3 by adding
1125 (**B**) vitamin B5 (pantothenic acid) at 125 µM which had no impact on cell size distribution; (**C**)
1126 quorum sensing peptide 1 (Qsp1p, 10µM) which significantly decreased cell size; (**D**)
1127 monoclonal anti-cryptococcal capsular polysaccharide antibodies E1 and 18B7 (at 166 µg/mL
1128 in MM) which significantly decreased cell size, as did fetal calf serum (FCS, 5%) (**E**), and
1129 phosphatidylcholine at 5mM (**F**). Fluconazole (**G**) and flucytosine (**H**) at concentration below
1130 the MIC (4 mg/L) drastically impaired TCs formation with no TCs produced upon drug
1131 exposure. (**I**) Step 1 was modified by subculturing H99O 8 times over one month on Sabouraud
1132 agar alone (Sub8), or supplemented with 20mg/L CFW (Sub8+CFW) or with 32mg/L
1133 fluconazole (Sub8+FLC). Compared to initial culture (0Sub), 8 sub-cultures (8Sub) decreased
1134 significantly the cell size (** p<0.0001, vs. 0Sub control, grey circled dots). In addition, iterative
1135 subcultures on CFW and FLC decreased and increased significantly the cell size compared to
1136 the 8Sub control, respectively. Median and IQR are shown in black for each condition (*
1137 p<0.0001 vs. 8Sub control, grey circled dots). The numbers above each condition represents

1138 the % of TCs observed. The experiments were performed in triplicate and pooled (mean cell
1139 counted ± SD = 2455±913).
1140
1141 **Fig 6. TCs generation is dependent on various genes *in vitro* and *in vivo*.**
1142 The different H99 strains harbored variable abilities to produce TCs compared to H99O (grey
1143 bar) with high TCs producer (H99O, S, L) and low TCs producer (KN99α, H99W, H99 CMO18)
1144 *in vitro* (**A**) and *in vivo* (**B**). *Sgf29Δ* and *lmp1Δ* deletion mutants show a decrease in TCs
1145 generation in various H99 backgrounds *in vitro* (**C**) and *in vivo* (**D**) compared to H99O. The ratio
1146 to the value obtained for H99O used as a calibrator in each experiment was calculated for
1147 each strain. Bar represent mean ± SD (mean cell counted=600). Khi2 test was performed to
1148 compare the experimental conditions to H99O, they were performed in triplicates and pooled
1149 (*p<0.0001).
1150
1151 **Fig 7. Non-synonymous mutation of *PKR1* enhances TCs generation based on clinical isolates**
1152 **analysis.**
1153 (**A**) Rim pathway is required for TCs generation *in vitro* in H99O (grey bar) and KN99a. (**B**) The
1154 screening of 56 *C. neoformans* serotype A MATα clinical isolates identified isolates AD2-06a
1155 (ratio=2.78) and AD2-02a (ratio=1.62) as TCs hyperproducers compared to H99O (grey bar);
1156 (**C**) Phylogenic tree were estimated using RAxML under the GTRCAT model of 29 clinical
1157 isolates. (**D**) Venn diagram representing the number of common or specific SNPs and Indel
1158 between AD2-06a, AD2-07 and AD3-55a. One of the AD2-06a specific SNPs is a non-
1159 synonymous mutation for *PKR1* (mutation Gly125fs); (**E**) Alignment of Pkr1 protein sequences
1160 from selected clinical isolates including H99O and AD2-07 that both harbor a wild type
1161 sequence. The Pkr1 domain architecture is formed by a dimerization domain in green (amino

1162 acids 2 to 40) and two cAMP binding site based on INTERPRO model in red (amino acids 219
1163 to 351 and 353 to 473). (**F**) Strains with *PKR1* loss-of-function mutation showed a variable
1164 ability to produce TC, as compared to H99O (grey bar). The clinical isolate AD2-07, which
1165 produces significantly less TCs was recovered from the CSF of an HIV-positive patient on day
1166 13 of amphotericin B treatment while AD2-06a, which produced the highest proportion of TC,
1167 was recovered from the initial CSF sample of the same patient. (**G**) The *pkr1Δ* mutant strain
1168 increased TCs formation compared to the parental strain KN99α. (*p<0.0001). The ratio to
1169 H99O, used as a calibrator in each experiment, was calculated for each strain (panel A, B, F
1170 and G) and results expressed as mean ±SD. Experiments A, F and G were done in triplicate, B
1171 only once (screening). To compare the experimental conditions to H99O, Khi2 analysis was
1172 performed (*p<0.0001, **p<0.05). Mean cell counted ± SD = 1165±528.
1173

1174 **Tables**

1175

1176 **Table 1: Genes affected by SNPs or Indels in the different H99 strains**

1177

Strains	Genes affected	Gene function	Genetic event
H99O	*CNAG_07634*	hypothetical	Deletion
	CNAG_04078	hypothetical	Insertion
	CNAG_06456	hypothetical	Insertion
H99S	*CNAG_07595*	hypothetical	Deletion/frameshift
	CNAG_12447	miscRNA	Insertion
	CNAG_12900	miscRNA	Insertion
H99L	CNAG_06392, *SGF29*	transcription factor (binds H3K4me2/3 and recruits histone deacetylation)	Deletion
KN99	CNAG_06392, *SGF29*	transcription factor (binds H3K4me2/3 and recruits histone deacetylation)	Deletion
H99W	*CNAG_06765*, *LMP1*	Hypothetical (involved in mating virulence and melanization)	Deletion/frameshift
H99 CMO18	*CNAG_06765*, *LMP1*	Hypothetical (involved in mating virulence and melanization)	Deletion/frameshift

1178

1179 **Table 2 – Alignment and SNP statistics of sequenced isolates using H99 as a reference**

1180

1181

Strain	MLST genotype	% of Assembly Covered by aligned reads	Alignment depth (X)	SNPs
AD3-55a	unique	100	133	28,070
AD2-06a	unique	100	129	28,202
AD2-07	unique	99	45	27,797
AD3-41a	unique	100	134	25,378
AD4-92a	A3/M3	100	132	11,906
AD4-47a	A4/M1	100	132	10,018
AD3-58	A4/M1	100	123	9,996
AD3-83a	A1/M1	100	166	172
AD2-99a	A1/M1	100	119	180
AD6-55a	related to A1/M1	100	108	12,440
AD6-54a	related to A1/M1	100	131	12,440
AD5-45a	related to A1/M1	100	142	12,417
AD1-95a	related to A1/M1	100	107	12,521
AD1-90a	related to A1/M1	100	122	12,511
AD5-67a	VNII	100	139	277,381
AD3-9a	VNII	100	111	277,417
AD3-11a	VNII	100	125	268,842
AD4-76a	Th	100	112	43,281
AD3-95a	Th	100	141	43,235
AD5-53a	A5/M5	100	130	42,291
AD2-82a	A5/M5	100	133	42,271
AD1-86a	A5/M5	100	105	43,778
AD5-39a	A4/M4	100	108	43,696
AD4-63a	A4/M4	100	129	43,736
AD2-04a	A4/M4	100	137	43,733
AD1-68a	A4/M4	100	132	43,778

1182

1183 **Table 3 : Clinical strains and mutations**

1184

Strains	Mutations
Ug2462	n.1333C>T|p.Arg445*|1333/1449
Bt117	n.1274_1280dupCTCTCCT|p.Asn428fs|1280/1449
Bt77	n.1293dupA|p.Arg432fs|1293/1449
8-1	n.878_911delCCGAGGGGAGCTCGTTTGGGGAGTTAGCGCTGAT|p.Ser293fs|911/1449
Bt58	n.742G>T|p.Glu248*|742/1449
AD2-06a	n.375_376delAG|p.Gly125fs|376/1449
Bt156	n.41dupA|p.Asp14fs|41/1449

1185

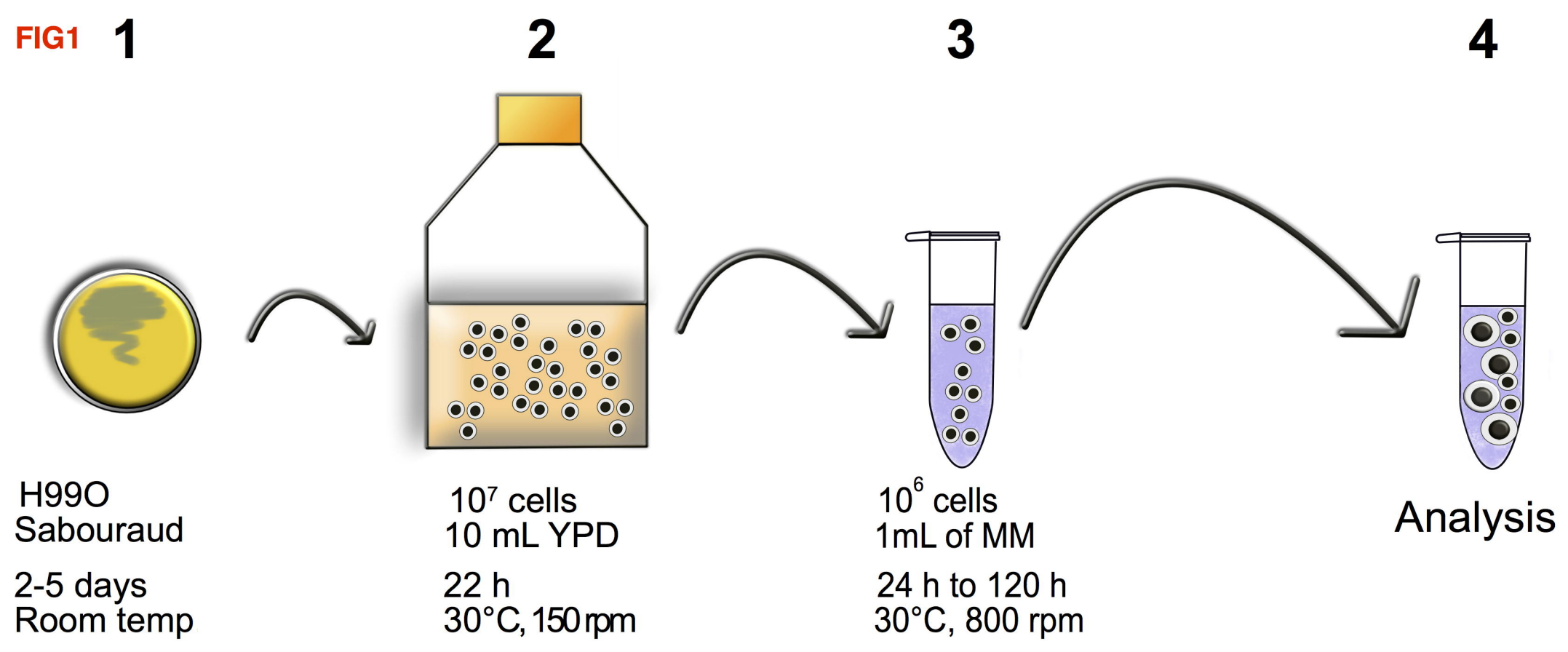
FIG1
1
2
3
4
H99O
Sabouraud
2-5 days
Room temp
10^7 cells
10 mL YPD
22 h
30°C, 150 rpm
10^6 cells
1mL of MM
24 h to 120 h
30°C, 800 rpm
Analysis

Fig2

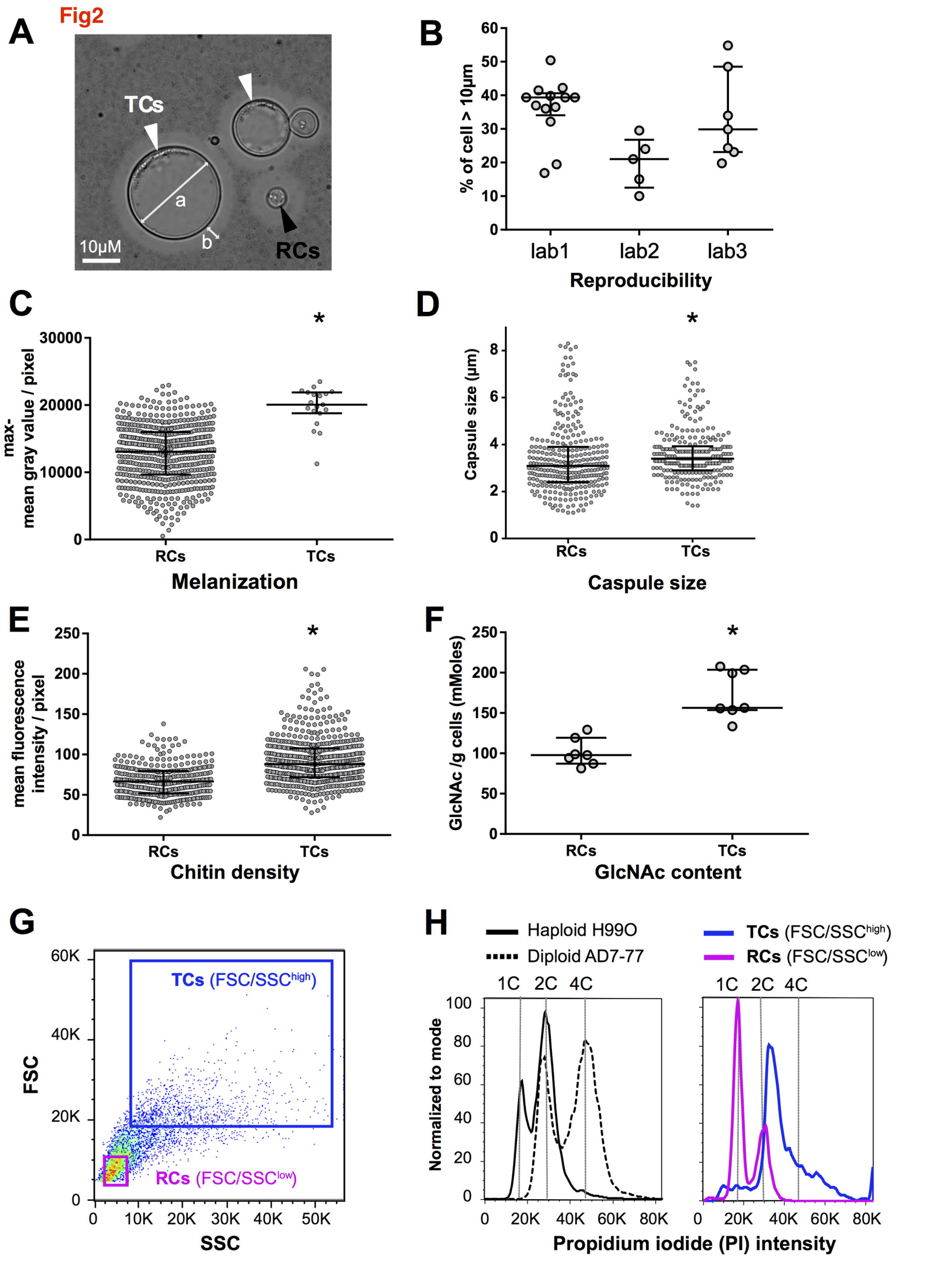
A
TCs
a
b
10μM
RCs
B
% of cell > 10μm
lab1
lab2
lab3
Reproducibility
C
max-mean gray value / pixel
RCs
TCs
Melanization
D
Capsule size (μm)
RCs
TCs
Caspule size
E
mean fluorescence intensity / pixel
RCs
TCs
Chitin density
F
GlcNAc /g cells (mMoles)
RCs
TCs
GlcNAc content
G
TCs (FSC/SSChigh)
RCs (FSC/SSClow)
FSC
SSC
H
Haploid H99O
Diploid AD7-77
TCs (FSC/SSChigh)
RCs (FSC/SSClow)
1C 2C 4C
Normalized to mode
Propidium iodide (PI) intensity

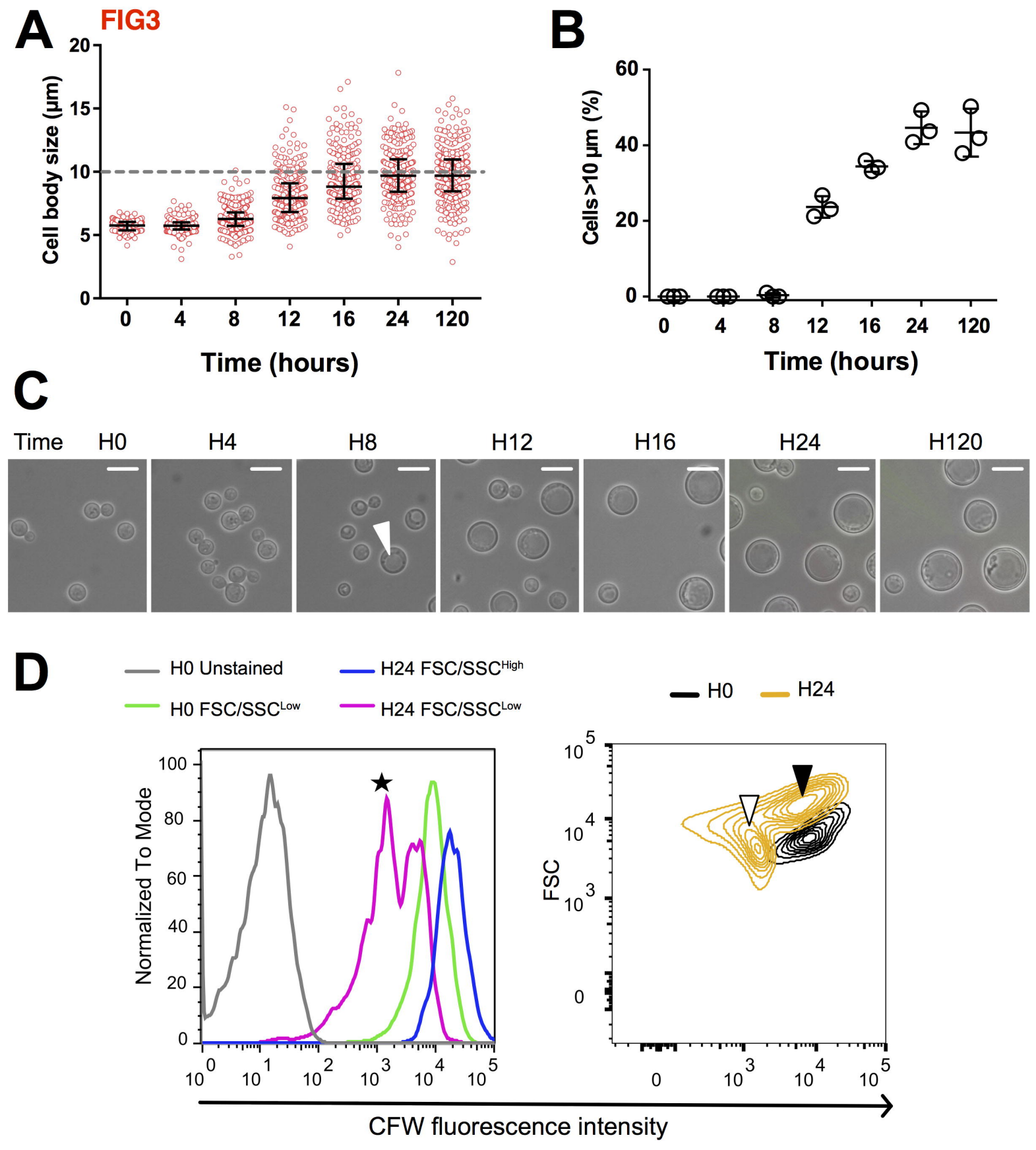
FIG3
A
Cell body size (µm)
Time (hours)
B
Cells>10 µm (%)
Time (hours)
C
Time
H0
H4
H8
H12
H16
H24
H120
D
H0 Unstained
H0 FSC/SSC^Low
H24 FSC/SSC^High
H24 FSC/SSC^Low
Normalized To Mode
CFW fluorescence intensity
H0
H24
FSC

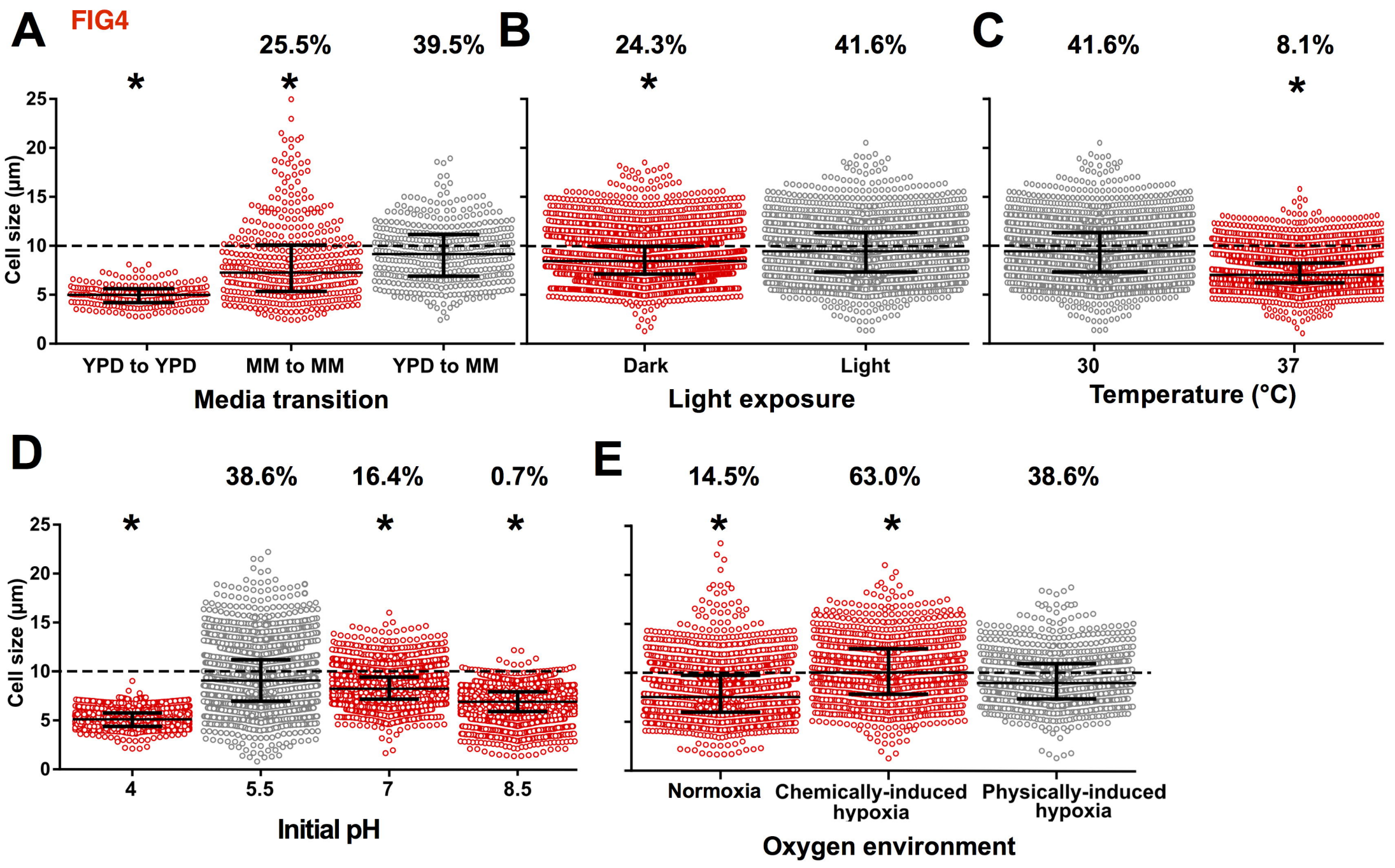
FIG4
A
25.5%
39.5%
*
*
Cell size (µm)
25
20
15
10
5
0
YPD to YPD
MM to MM
YPD to MM
Media transition
B
24.3%
41.6%
*
Dark
Light
Light exposure
C
41.6%
8.1%
*
30
37
Temperature (°C)
D
38.6%
16.4%
0.7%
*
*
*
4
5.5
7
8.5
Initial pH
E
14.5%
63.0%
38.6%
*
*
Normoxia
Chemically-induced hypoxia
Physically-induced hypoxia
Oxygen environment

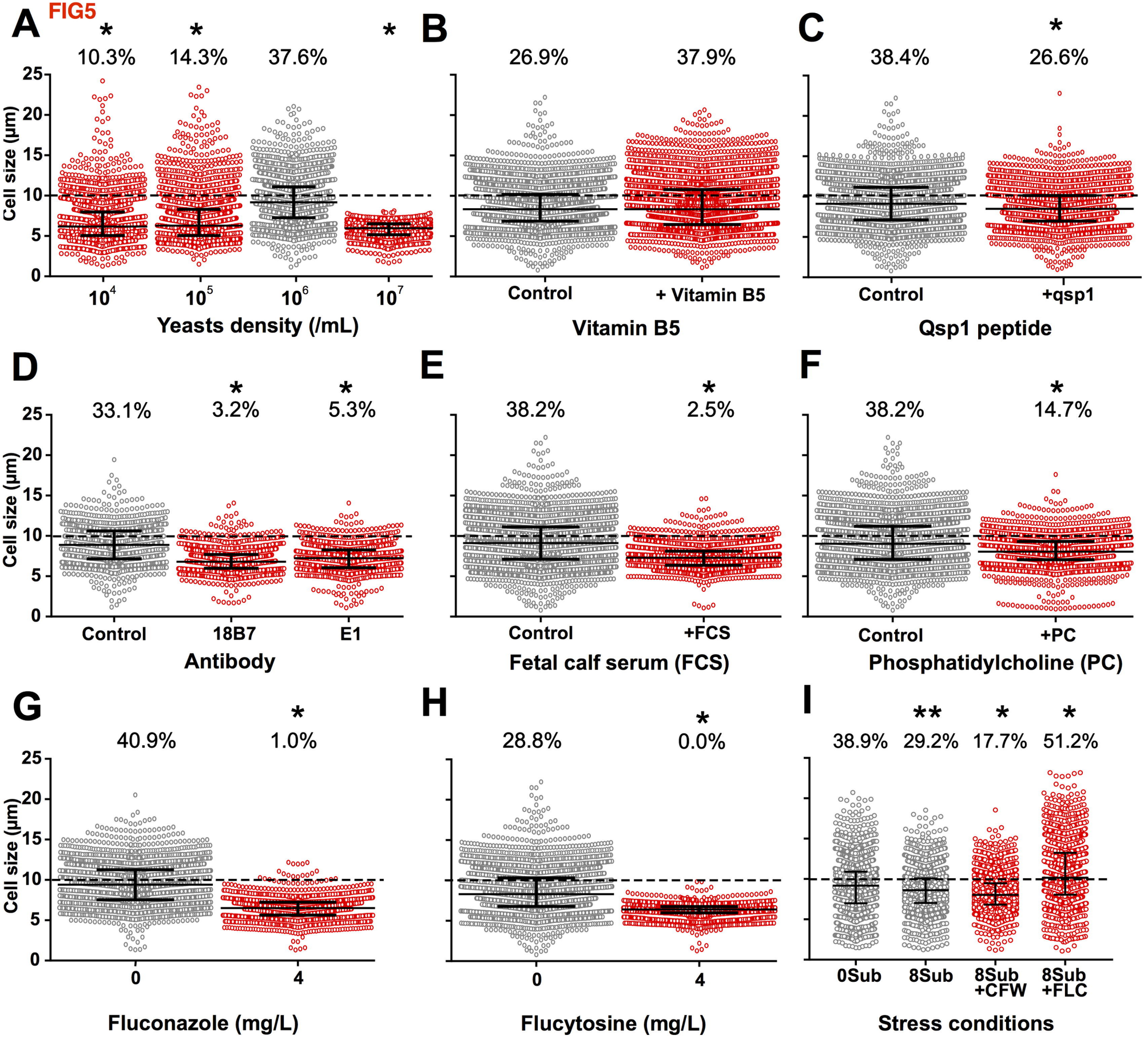
FIG5
A
B
C
D
E
F
G
H
I
Cell size (µm)
10.3%
14.3%
37.6%
Yeasts density (/mL)
26.9%
37.9%
Control
+ Vitamin B5
Vitamin B5
38.4%
26.6%
Control
+qsp1
Qsp1 peptide
33.1%
3.2%
5.3%
Control
18B7
E1
Antibody
38.2%
2.5%
Control
+FCS
Fetal calf serum (FCS)
38.2%
14.7%
Control
+PC
Phosphatidylcholine (PC)
40.9%
1.0%
Fluconazole (mg/L)
28.8%
0.0%
Flucytosine (mg/L)
38.9%
29.2%
17.7%
51.2%
0Sub
8Sub
8Sub +CFW
8Sub +FLC
Stress conditions

Fig6

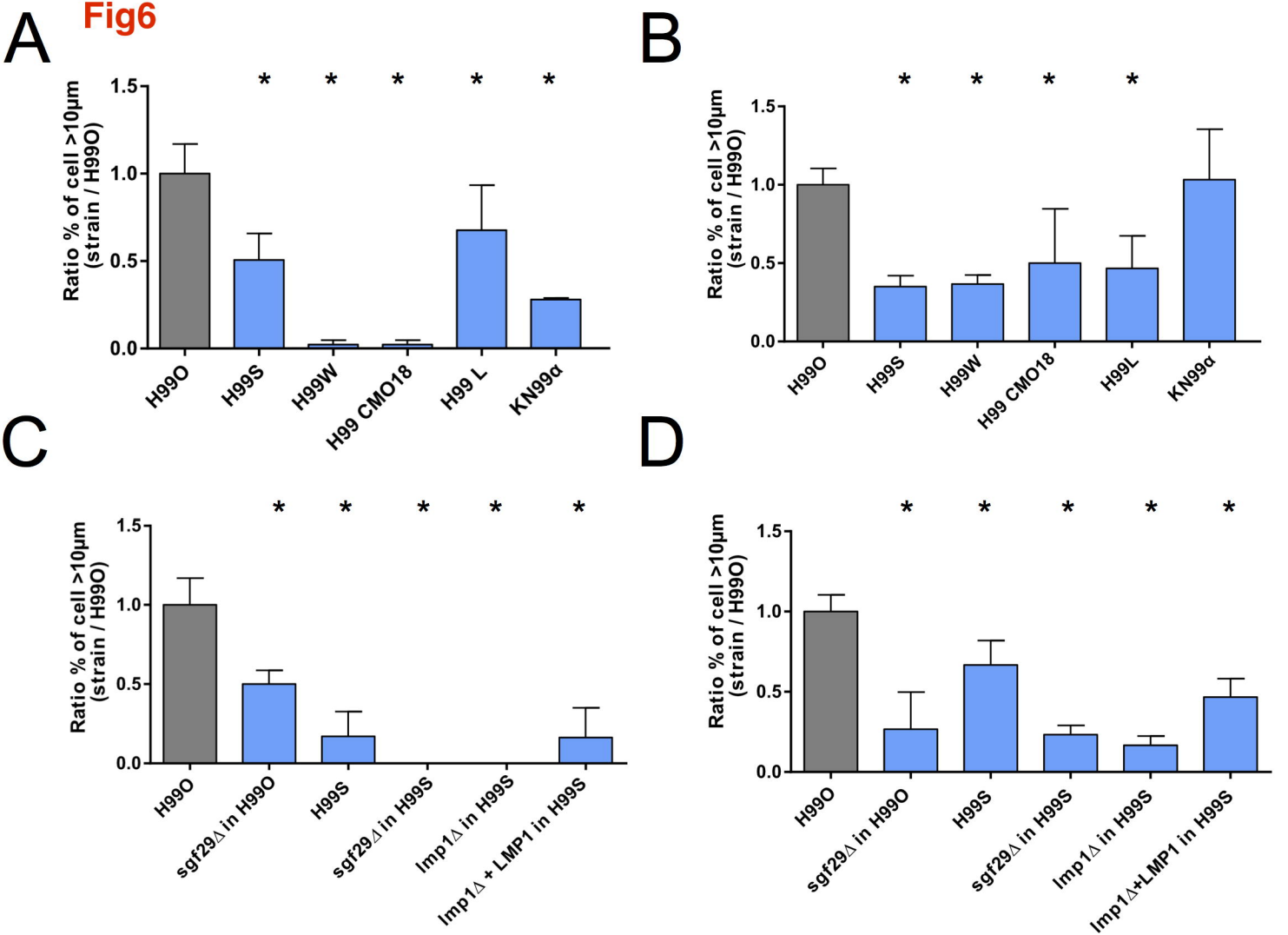
A
B
C
D
Ratio % of cell >10µm (strain / H99O)
1.5
1.0
0.5
0.0
*
H99O
H99S
H99W
H99 CMO18
H99 L
KN99α
H99L
sgf29Δ in H99O
sgf29Δ in H99S
Imp1Δ in H99S
Imp1Δ + LMP1 in H99S
Imp1Δ+LMP1 in H99S

Fig7

A

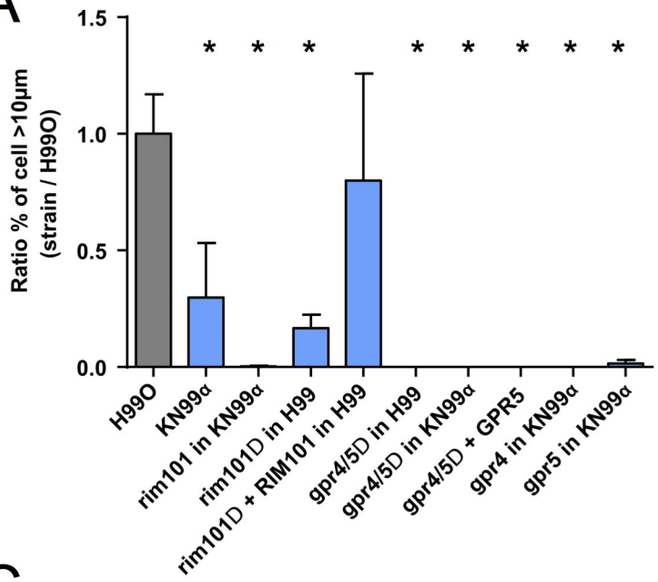

B

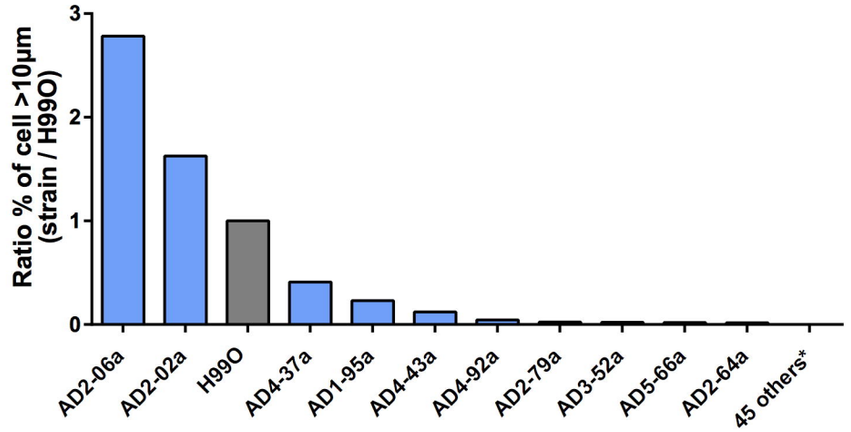

C

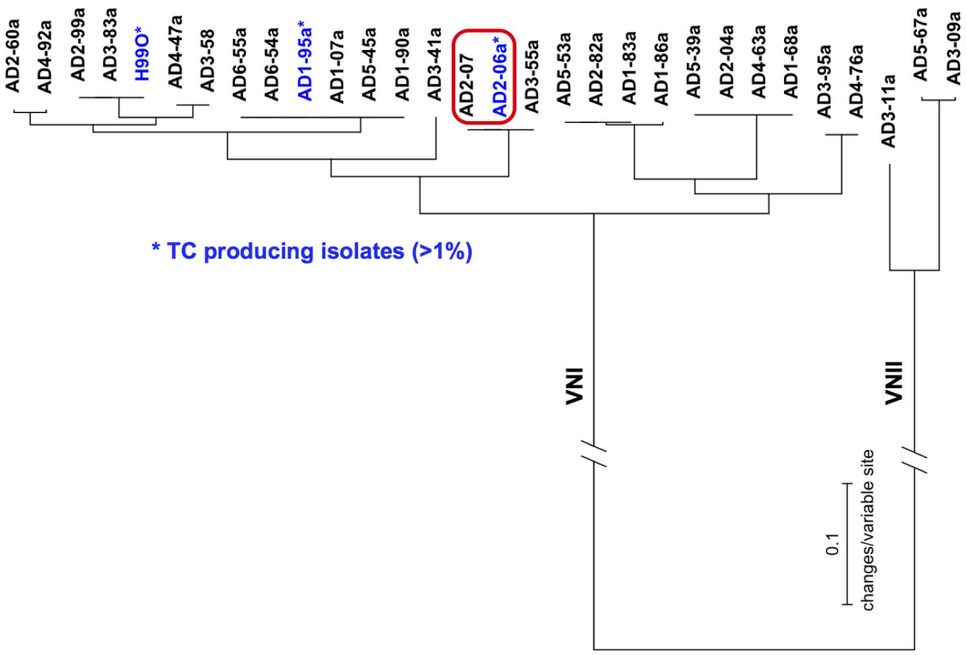

D

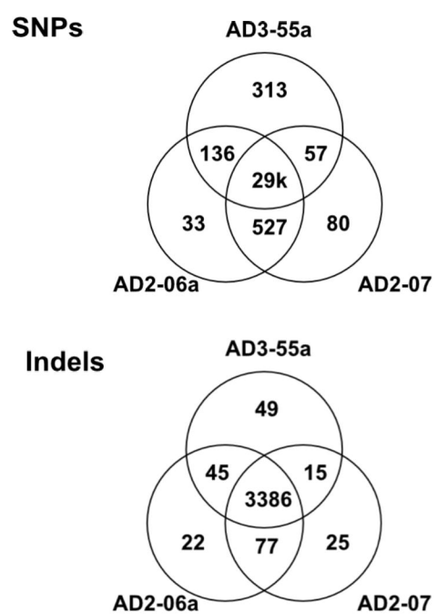

E

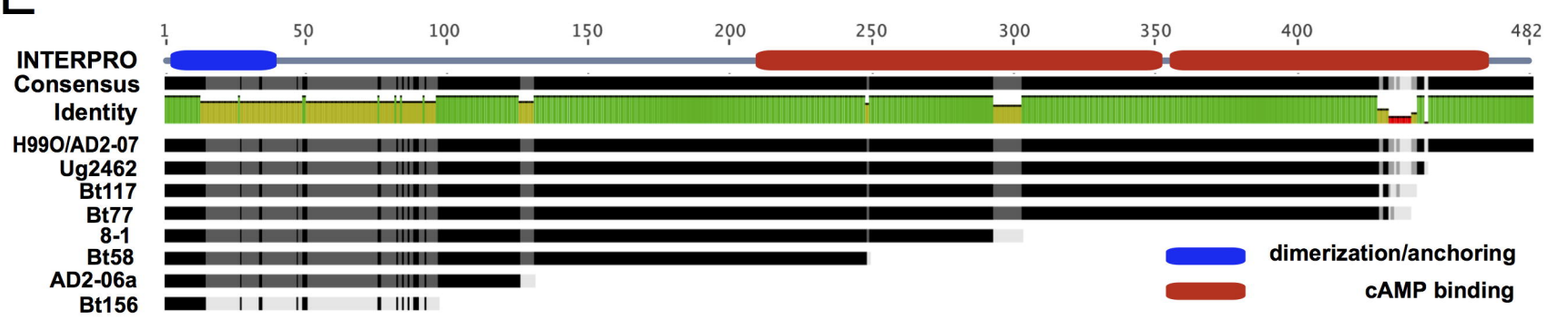

F

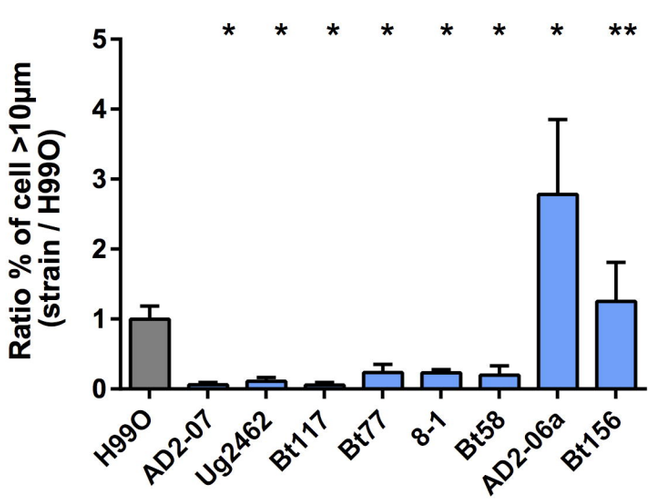
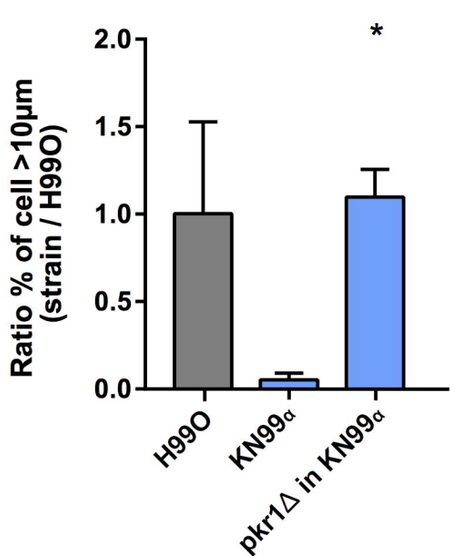
G